GEORG-AUGUST-UNIVERSITÄT
GÖTTINGEN IN PUBLICA COMMODA SEIT 1737

DLR

Master's Thesis

Development of a polyatomic particle Fokker-Planck method for modeling of rarefied gas flows based on direct modeling

prepared by

Aaron Nagel

from Bad Karlshafen

at the German Aerospace Center
Institute of Aerodynamics and Flow Technology
Spacecraft Department in Göttingen

Thesis Period:	1st June 2023 until 12th October 2023
Supervisor:	Dr. Martin Grabe
First Referee:	Prof. Dr. rer. nat. Dr. habil. Andreas Dillmann
Second Referee:	Prof. Dr. Martin Rein

Abstract

To provide a significant speedup in modeling rarefied gas flows, the collision operator in the Boltzmann equation is approximated by a Fokker-Planck operator in velocity space. A polyatomic extension of the diatomic direct modeling approach in the Fokker-Planck framework is carried out in this thesis. The model extension is verified by a code to code comparison, using DSMC data of the *SPARTA* code and *PICLas* code. Diatomic tests are performed using N_2 and polyatomic tests using CO_2. Temperature relaxation tests also include CH_4 tests to show the capability of predicting the correct temperatures for degenerate energy modes, such as they occur in vibrtional modes in CH_4.
The model is verified by heat bath tests to show correct temporal relaxation into equilibrium temperatures for diatomic and polyatomic species. Two dimensional hypersonic flow tests around a cylinder investigate the particle number density as well as thermal and internal temperatures of the flow field. The relaxation of the energy for different timestep sizes and runtime efficiency for small Knudsen numbers are investigated.
The diatomar relaxation process of translational and internal temperatures using N_2 show very good agreement with the reference data and theoretical prediction. The polyatomic relaxation processes of the temperatures are investigated using CO_2 and CH_4. All relaxation tests predict the equilibrium temperature and temporal relaxations accurately.
Further tests investigate the flow fields of a hypersonic flow around a cylinder by 2D simulations. The direct Fokker-Planck modeling is compared with DSMC and a FP master equation approach. The particle number density field and the temperature field is analyzed with investigations on translational, rotational and vibrational energies. The diatomic flow fields show only small deviations. The polyatomic extension approximates the shock and the overall flow field well, but shows deviations in the wake region, where the flow is rarefied. The FP direct model may be improved for rarefied regions in future works but in the context of a hybrid coupling, these regions may not use the FP direct model anyway. Finally, investigations of runtime improvements of the new modeling are made by showing a computationally more efficient model for smaller Knudsen numbers and the ability to resolve the temporal relaxation with larger timestep sizes very accurately.

Contents

List of Figures

Nomenclature

Latin letters

Variable	Meaning	Unit
A	velocity drift coefficient	$\mathrm{m} \cdot \mathrm{s}^{-2}$
d_{ref}	reference diameter of particle	m
d_{rot}	rotational degrees of freedom	–
d_{vib}	vibrational degrees of freedom	–
D	velocity diffusion coefficient	$\mathrm{m} \cdot \mathrm{s}^{-3/2}$
e	mass specific energy	$\mathrm{J} \cdot \mathrm{kg}^{-1}$
E	energy	J
f	probability density function	–
F	external acceleration	$\mathrm{m} \cdot \mathrm{s}^{-2}$
g	number of degeneracy	–
$\mathcal{H}$	phase space	–
I	moment of inertia	$\mathrm{kg} \cdot \mathrm{m}^2$
J	number of vibrational modes	–
k_B	Boltzmann constant	$\mathrm{J} \cdot \mathrm{K}^{-1}$
Kn	Knudsen number	–
l	characteristic size	m
m	mass of a particle	kg
Ma	Mach number	–
n	particle number density	m^{-3}
p	pressure	$\mathrm{N} \cdot \mathrm{m}^{-2}$
P	probability	–
$\mathcal{Q}$	partition function	–
R	rate coefficient of master equation ansatz	s^{-1}
S	collision operator	s^{-1}

Variable	Meaning	Unit
t	time	s
T	temperature	K
T_{ref}	reference temperature	K
T_{rot}	rotational temperature	K
T_{th}	thermal temperature	K
T_{vib}	vibrational temperature	K
v	translational velocity	$\mathrm{m} \cdot \mathrm{s}^{-1}$
v'	thermal velocity	$\mathrm{m} \cdot \mathrm{s}^{-1}$
v_{rot}, Ω	rotational velocity	$\mathrm{m} \cdot \mathrm{s}^{-1}$
v_{vib}, Ξ	vibrational velocity	$\mathrm{m} \cdot \mathrm{s}^{-1}$
V	volume	m^3
W	standard normal variates	–
x	position vector coordinate	m
Z	collision number	–

Greek letters

Variable	Meaning	Unit
β	Boltzmann factor	J^{-1}
θ	characteristic temperature	K
λ	mean free path	m
μ	viscosity	$\mathrm{N} \cdot \mathrm{s} \cdot \mathrm{m}^{-2}$
ν	mean collision frequency	s^{-1}
ξ_i	vibrational velocity component	$\mathrm{m} \cdot \mathrm{s}^{-1}$
Ξ	vibrational velocity vector	$\mathrm{m} \cdot \mathrm{s}^{-1}$
ρ	mass density	$\mathrm{kg} \cdot \mathrm{m}^{-3}$
τ	relaxation time	s
τ_{coll}	mean collision time	s
ψ	DLB weighting function	–
Ψ	combining translational and internal velocity vector	$\mathrm{m} \cdot \mathrm{s}^{-1}$
ω	viscosity exponent	–
ω_i	rotational velocity component	$\mathrm{m} \cdot \mathrm{s}^{-1}$
Ω	rotational velocity vector	$\mathrm{m} \cdot \mathrm{s}^{-1}$

Indices

Index	Meaning
∞	free stream condition
Boltz	Boltzmann pairwise collision description
FP	Fokker-Planck collision description
coll	collision
conti	continuous
disc	discrete
el	elastic
eq	equilibrium
inel	inelastic
int	internal
ref	reference values for a fixed set of parameters
rot	rotation
th	thermal
tot	total
tr	translation
vib	vibration

Abbreviations

Abbreviations	Meaning
CFD	computational fluid dynamics
CLT	continuous Landau-Teller
DLB	discrete Larsen-Borgnakke
DLT	discrete Landau-Teller
DSMC	Direct Simulation Monte Carlo
EUCASS	European Conference for Aerospace Sciences
FP	Fokker-Planck
LT	Landau-Teller
PICLas	Plasma Particle-In-Cell Kinetic Code of the Universtity of Stuttgart
SPARTA	Stochastic PArallel Rarefied-gas Time-accurate Analyzer

Abbreviations	**Meaning**
VHS/VSS	Variable hard sphere / variable soft sphere

1. Introduction

The modeling of gas flows around reentry vehicles or jet plume expansion into vacuum faces a large range of Knudsen numbers [13]. The Knudsen number Kn characterizes rarefaction of a gas by the ratio of the mean free path λ of a particle to the characteristic length scale l by $Kn \equiv \lambda/l$. For small Knudsen numbers, many particle collisions occur so the velocities of the particles are in near thermal equilibrium and the gas can be modeled as a continuum using the Navier-Stokes equations. Large Knudsen numbers lead to non-equilibrium and the evolution of the particles velocity distribution needs to be modeled.
Rarefied flows can be described by the Boltzmann equation that determines the dynamics of the system by the evolution of a probability density function in phase space. With Birds DSMC method [5], the Boltzmann equation can be solved accurately. However, the computational expenses become too large for small Knudsen numbers due to the complexity of the Boltzmann collision operator which leads to the necessity to model a large number of collisions. A coupling of a solver combining the modeling of the Boltzmann equation by DSMC and the Navier-Stokes equation is generally a difficult task. This is because of the fluctuating boundary conditions for the Navier-Stokes solver, which is caused by the stochastic behaviour of the DSMC method [11]. Therefore, the complex collision operator in the Boltzmann equation is approximated by a Fokker-Planck (FP) operator in velocity space to reduce the computational cost for small Knudsen numbers while maintaining the particle approach [11]. DSMC models pairwise collisions, whereas the FP operator models the collisions by local drift and diffusion coefficients that are matched to reproduce the production terms of the Boltzmann collision operator in the continuum limit [10]. Both methods use computational particles. This way, a hybrid modeling approach can be set up where FP can be used in regions of high densities and small Knudsen numbers, while DSMC is used for rarefied flow regions and large Knudsen numbers [8]. DSMC requires to resolve the mean free path, which can be difficult for small Knudsen numbers, as will be discussed in section 4.3.1. Besides the aim of an im-

provement in runtime, the FP modeling also looses this spatial restriction. Further, temporal restrictions are able to be loosened as well, as section 4.3.2 investigates.

The goal of the FP modeling is the hybrid coupling with DSMC to switch between the different collision models within a simulation to increase the runtime efficiency and use less strict resolution criteria. As can be seen in figure 1.1, the flow field of, for example, a reentry vehicle may range from continuum free stream flow to a rarefied region in the wake. To avoid combining continuum Navier-Stokes solvers and particle methods, the FP method should be used to efficiently model dense regions even with a particle method and model rarefied regions accurately using DSMC.

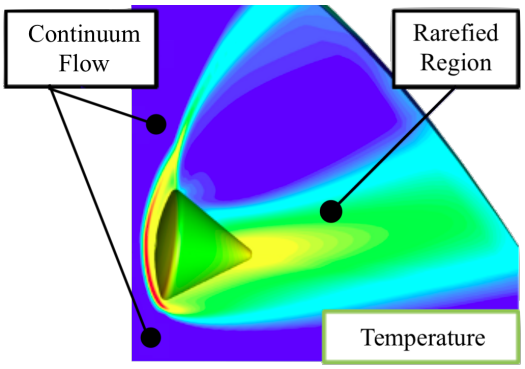

Figure 1.1.: Temperature field of a reentry vehicle in near continuum-rarefied transition regime from Craft Tech [21].

This thesis will be focusing on the energy distribution of translational and internal modes, i.e. rotational and vibrational modes, within a Fokker-Planck approximation of the collision term in the Boltzmann-equation. In contrast to monatomic gas flows, polyatomic molecules can take up a significant amount of energy in internal modes like rotation and vibration, which have a large influence on the entire flow field [12]. The different energy modes generally show very different relaxation times and may be modeled on continuous or discrete energy scales [12]. An extension of the FP operator to a diatomic modeling has been proposed in the literature, e.g by the Master-equation ansatz [12], a direct modeling approach [6] or by Mathiaud et al. [16].
An extension of the direct modeling approach [6] to polyatomic gas is carried out in this thesis, parts of which have already been published in the EUCASS paper [18]. Improvements to these previously published results are archived, for example by integrating a translational velocity scaling factor in section 3.8. This factor guarantees exact total energy conservation in each timestep instead of a fluctuating total

energy that is only conserved on average. Following the theoretical setup in section 2 and modeling approach in section 3, the new model is investigated in section 4 to validate the accuracy of correct relaxation, flow structures in hypersonic 2D flows and its efficiency for small Knudsen numbers and larger timesteps.

Disclaimer: Additional publication

Parts of this Master's thesis have already been published at the European Conference for Aerospace Sciences 2023 (EUCASS) in a conference paper by the author [18], literally and figuratively. In particular, the modeling of kinetic gases within the Fokker-Planck approach in section 3, including the results of the proposed extension to the polyatomic model are published in the corresponding paper. The verification chapter includes results that differ from the paper, due to improvements that have been done in the meantime.

2. Kinetic theory of gases

In aerothermodynamics, the modeling of rarefied gas flows is an important part of the large range of different flow regimes that a spacecraft faces. For a decreasing density, the average distance of a particle between two collisions with other particles increases. Using the *Variable Hard Sphere* mode (VHS), this distance is defined as the mean free path and given by [5]

$$\lambda = \frac{1}{\sqrt{2}\pi d_{\text{ref}}^2 n \left(\frac{T_{\text{ref}}}{T}\right)^{\omega-1/2}}, \tag{2.1}$$

with the particles reference diameter d_{ref}, the particle number density n, temperature T, reference temperature T_{ref} and viscosity exponent ω. The mean free path becomes large compared to the characteristic problem size l for very dilute gases. The relation defines the *Knudsen number*

$$Kn = \frac{\lambda}{l}, \tag{2.2}$$

which can be used to characterize the flow regime. The continuum regime where the *Navier-Stokes* equation hold is characterized by $Kn \lesssim 0.1$ [1, 5], while the flow for Knudsen numbers of $Kn > 10$ is typically considered as free molecular with no collisions [1].
In a flow with a small Knudsen number, a small mean free path and a small collision time, that is defined as the average time between two collisions, result in a large number of collisions per time which keeps the distribution of the thermal velocities close to a Maxwellian distribution [12]. For these flow regimes, equilibrium assumptions hold and the Navier-Stokes equations can be used. If on the other hand the Knudsen number is large, collisions are rare and the velocity distribution remains off the equilibrium for a significantly long time and continuum can not be assumed anymore [12].

To model non-equilibrium flows where continuum can not be assumed anymore,

the flow needs to be modeled by studying the velocity distribution and its evolution in time.
Considering a gas where each molecule has a velocity $\mathbf{v}(t)$ and a position $\mathbf{x}(t)$ at time t, the statistics of particles in a gas is described by the probability velocity density function $f(\mathbf{v}, \mathbf{x}, t)$ [12]. Its evolution described by the *Boltzmann* equation covered in section 2.1, has to be evaluated to model the dynamics of the system.
The *Boltzmann* equation is generally capable of describing the system over the whole Knudsen range but its solution is computationally infeasible for particle methods once the Knudsen number becomes small because too many collisions and too small scales need to be resolved [8]. Thus one has to choose a suitable model for the problem of interest. An overview of the validity range of the different model approaches is given in figure 2.1.

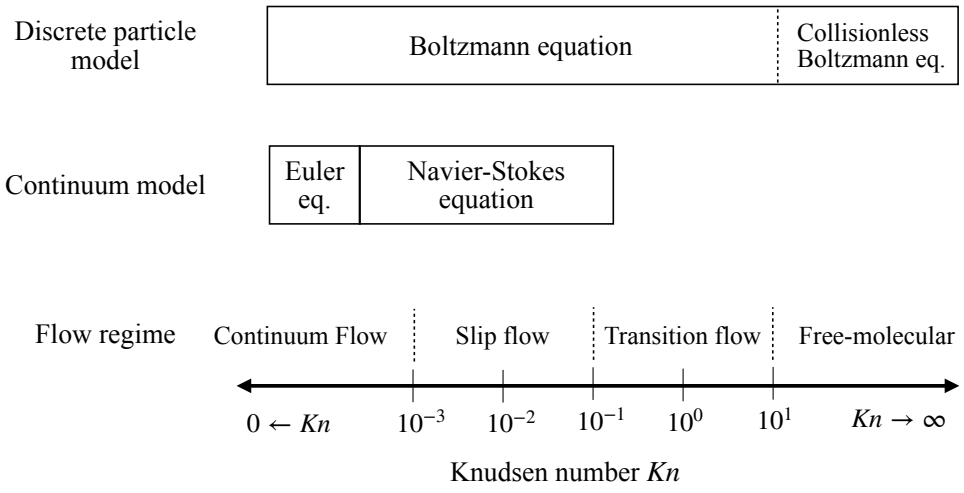

Figure 2.1.: Overview of the validity range of the different models over the Knudsen number range adopted from [1, 22].

2.1. Boltzmann equation

The evolution in time of the system is given by the motion of the velocity distribution function f in phase space $\mathcal{H}$, which is a probability density function. To gain the governing equation of the systems dynamic, the possible change of the function of state on one side of the equation must balance with the cause of the change on the other side of the equation.

On one side of the equation, the changes that can happen to the function f are collected, which result from the total differential of the function $f(\mathbf{v}, \mathbf{x}, t)$. These can be explicit changes in time, convectional changes and changes due to a velocity change. On the other side of the equation, further causes of the changes are collected. In the statistical description of a particle ensemble, changes of the velocity distribution function can also happen by collisions. This collision term is often referenced as *collision operator*. Taking all together, the equation determining the dynamics of the system is called *Boltzmann* equation and using Einstein's index summation notation, it reads

$$\frac{\partial f}{\partial t} + v_i \frac{\partial f}{\partial x_i} + F_i \frac{\partial f}{\partial v_i} = \underbrace{\left(\frac{\partial f}{\partial t}\right)_{\text{coll}}}_{S_{\text{coll}}(f)}, \tag{2.3}$$

where F_i is an external acceleration that is assumed to be independent of the velocity. Finding an accurate and reasonable description of the particle collision term on the right hand side is the challenge of modeling the dynamics. A precise collision term for binary collisions is given by the *Boltzmann* collision operator [8]

$$\left(\frac{\partial f}{\partial t}\right)_{\text{Boltz}} = \int_{\mathbb{R}^3} \int_0^{4\pi} (f(\mathbf{v}'_{\text{A}}) f(\mathbf{v}'_{\text{B}}) - f(\mathbf{v}_{\text{A}}) f(\mathbf{v}_{\text{B}})) g I(\Omega, g) \mathrm{d}\Omega \mathrm{d}\mathbf{v}_{\text{B}}, \tag{2.4}$$

where $g = |\mathbf{v}_{\text{A}} - \mathbf{v}_{\text{B}}|$ is the relative velocity of the two colliding particles, $I(\Omega, g)$ is the differential cross section, $(\mathbf{v}'_{\text{A}}, \mathbf{v}'_{\text{B}})$ are the post collisional velocities of the particle velocities $(\mathbf{v}_{\text{A}}, \mathbf{v}_{\text{B}})$, and the integrals are the solid angle integral $\int \mathrm{d}\Omega$ around g and the velocity integral. The collisions described by this collision operator so far covers only elastic collision. Obviously, once there are inelastic collisions, the model has to be extended by states that can take up the energy difference resulting from inelastic collisions. For now, the system will be set up by elastic considerations and an extension will be done in further sections.

The direct solution of this stochastic integro-differential equation is a computationally expensive task [14]. Modeling the Boltzmann collision operator is generally demanding. Therefore, a more efficient approximation of the collision operator will be set up by the Fokker-Planck (FP) operator in section 3.1 and the *Direct-Simulation-Monte-Carlo* method (DSMC) in section 3.3 is used to model a discrete subset of particles representing the distribution of the velocity distribution function.

2.2. Energy distribution of molecules in a gas

2.2.1. Phase space and degrees of freedom

This section briefly derives thermodynamic and statistical physics relations following *Balian* [3], that are needed in further sections to formulate the modeling method.
The state of a particle typically is characterized by the d coordinates of its phase space $\mathcal{H} \subseteq \mathbb{R}^d$. So the energy E of a particle generally may depend on its d degrees of freedom, each represented by one of the coordinates in phase space. Usually these coordinates are the three spatial coordinates and three momentum coordinates $(\vec{x}, \vec{p}) \in \mathbb{R}^6$, but in this work they will include also additional coordinates for rotational and vibrational states $(\vec{x}, \vec{p}, \vec{\Omega}, \vec{\Xi}) \in \mathbb{R}^{d_{\text{tot}}}$, with $d_{\text{tot}} = 6 + d_{\text{rot}} + d_{\text{vib}}$ where d_{rot} and d_{vib} are discussed further down in this sections. If an ensemble of N particles is considered, the phase space generally gets expanded to $N \cdot d_{\text{tot}}$ dimensions, which is worth mentioning but not needed at this point.
The number of translational degrees of freedom is given by the spacial dimensions that the particle can move along. If particles can change their position in three spacial dimensions, the translational degree of freedom is $d_{\text{tr}} = 3$. If the particle can move in only fewer dimensions, the translational degree of freedom adjusts accordingly.
The number of rotational and vibrational degrees of freedom d_{rot} depends on the shape of the molecule. Molecules generally can rotate around the three rotational axis, where each of them may contain rotational energy. For linear molecules, only two of the rotational axis contain rotational energy. So the number of rotational degrees of freedom is $d_{\text{rot}} = 3$ for irregularly shaped molecules and $d_{\text{rot}} = 2$ for linear molecules.
The number of vibrational degrees of freedom d_{vib} depends on the number of atoms in the molecule. Each vibrational mode j contributes to the total energy with two degrees of freedom in phase space, namely kinetic and potential energy. So the number of vibrational degrees of freedom is $d_{\text{vib}} = 2J$. N individual pointlike atoms generally have $3N$ degrees of freedom[3], or likewise $3N$ translational modes, that contain the total energy. Therefore, the number of vibrational modes of a molecule with N atoms is $J = 3N - d_{\text{tr}} - d_{\text{rot}}$, which results in:

$$J = \begin{cases} 3N - 5 & \text{linear molecule} \\ 3N - 6 & \text{non-linear molecule.} \end{cases} \tag{2.5}$$

The energy of the different modes may be treated differently, depending on their distribution of the energy on continuous or discrete energy scales, which is discussed in further sections.

2.2.2. Discrete and continuous energy scales

To calculate the energy E of a particle, the different possible energy states E_n with probability P_n of the particle need to be covered. Assuming a Boltzmann distribution, the probability of a particle being in state n is given by [3]

$$P_n(E_n) = \frac{1}{\mathcal{Q}} e^{-\beta E_n}, \tag{2.6}$$

where $\beta = 1/(k_B T)$ with the Boltzmann constant $k_B = 1.38 \cdot 10^{-23}\mathrm{J/K}$ and the partition function $\mathcal{Q}$. The partition function covers discrete energy levels E_n by [3]

$$\mathcal{Q}_{\mathrm{disc}} = \sum_{n=0}^{\infty} e^{-\beta E_n} \Leftrightarrow E_n \text{ equidistant: } \mathcal{Q}_{\mathrm{disc}} = \frac{1}{1 - \exp(-\beta E)}. \tag{2.7}$$

Thus, the average energy of the discrete energy states is given by [3]

$$\langle E \rangle = \sum_{n=0}^{\infty} E_n P_n(E_n) = -\frac{1}{\mathcal{Q}} \frac{\partial \mathcal{Q}}{\partial \beta} = -\frac{\partial \ln(\mathcal{Q})}{\partial \beta}, \tag{2.8}$$

which can be evaluated by the partition function directly. Similarly, on a continuous energy scale, the probability is given by $P(E) = \exp(-\beta E)/\mathcal{Q}_{\mathrm{conti}}$ with the partition function of a continuous energy E, replacing the sum by an integral in equation (2.7)

$$\mathcal{Q}_{\mathrm{conti}} = \int_0^{\infty} \mathrm{d}E \; e^{-\beta E}, \tag{2.9}$$

and the average energy is given by $\langle E \rangle = \int E \; P(E) \mathrm{d}E$.

2.2.3. Equipartition theorem

Considering a specific energy on a continuous scale that depends on d of the total number of d_{tot} degrees of freedom, the dependencies read $E = E(x_1, ..., x_d)$, where the x_i are arbitrary variables whose change contribute to a change of E. If we further assume that each degree of freedom contributes independently of all other degrees of freedom to the total energy, the energy can be written as the sum of the

individual energies $E_i = E_i(x_i)$

$$E = \sum_{i=1}^{d} E(x_i). \tag{2.10}$$

To set up the continuous partition function, all possible energy states arising from x_i need to be considered. While the energy itself remains positive, its values may come from variables x_i that may be positive or negative, so the partition function integral from equation (2.9) can be written as

$$\mathcal{Q}_{\text{conti}} = \int_{-\infty}^{\infty} \exp(-\beta \sum_{i=1}^{d} E(x_i)) \mathrm{d}x_1 ... \mathrm{d}x_d = \int_{-\infty}^{\infty} \prod_{i=1}^{d} \exp(-\beta E(x_i)) \mathrm{d}x_i. \tag{2.11}$$

Taking advantage that the energy by each degree of freedom is independent of all other states $x_i \neq x_i(x_{i \neq j})$, the integral of the product can be written as the product of the integrals

$$\mathcal{Q}_{\text{conti}} = \prod_{i=1}^{d} \int_{-\infty}^{\infty} \exp(-\beta E(x_i)) \mathrm{d}x_i \underset{(2.9)}{=} \prod_{i=1}^{d} \mathcal{Q}(E_i), \tag{2.12}$$

which means that the total partition function is the product of the partition function of each individual degree of freedom.
If we can further assume that the energy scales quadratically with x_i (assume $E_i \sim cx_i^2$), the functions $\mathcal{Q}(E_i)$ can be evaluated using the *Gaussian integral*

$$\mathcal{Q}(E_i) = \int_{-\infty}^{\infty} e^{-\beta E_i} \mathrm{d}x_i = \int_{-\infty}^{\infty} e^{-\beta c x_i^2} \mathrm{d}x_i \underset{\text{Gauss}}{=} \left(\frac{\pi}{\beta c} \right)^{\frac{1}{2}}. \tag{2.13}$$

This can be used to calculate the average energy resulting from x_i, which due to their independencies is the average energy per degree of freedom

$$\langle E \rangle_i = -\frac{\partial \ln \mathcal{Q}(x_i)}{\partial \beta} = \frac{1}{2\beta} = \frac{1}{2} k_B T. \tag{2.14}$$

So the average of a continuous energy results in

$$\begin{aligned} \langle E \rangle &= -\frac{\partial \ln \mathcal{Q}(x)}{\partial \beta} \underset{(2.12)}{=} -\frac{\partial \ln(\prod_{i=1}^{d} \mathcal{Q}(E_i))}{\partial \beta} = -\frac{\partial}{\partial \beta} \sum_{i=1}^{d} \ln \mathcal{Q}(x_i) \\ &= \sum_{i=1}^{d} -\frac{\partial}{\partial \beta} \ln \mathcal{Q}(x_i) \underset{(2.14)}{=} \sum_{i=1}^{d} \langle E \rangle_i \underset{(2.14)}{=} \sum_{i=1}^{d} \frac{1}{2} k_B T = \frac{d}{2} k_B T. \end{aligned} \tag{2.15}$$

2.2.4. Discrete equidistant energy levels

In the special case of discrete energy levels E_n with equidistant spacing $\Delta E = E_n - E_m = \text{const}$, $\forall m \neq n$, the partition function can be evaluated explicitly as shown in equation (2.7). Assuming that each mode is independent and therefore contributes to the overall energy independently, the partition function is the product of each individual partition function of mode j (see p. 573 in [2]), while raising to the power of degeneracy g_j of the j'th mode to cover multiple occurrence of mode j

$$\mathcal{Q}_{\text{disc}} = \prod_{j=1}^{J} \left(\frac{1}{1 - \exp(-\beta E_j)} \right)^{g_j}. \tag{2.16}$$

Therefore, the average energy using $\mathcal{Q}_{\text{disc}}$ in (2.8) results in

$$\langle E \rangle_{\text{disc}} = \sum_{j=1}^{J} \frac{g_j \cdot E_j}{\exp(\beta E_j) - 1}. \tag{2.17}$$

2.2.5. Internal energies

To calculate the internal energy of polyatomic gases, the partition function for polyatomic energies needs to be evaluated and the average energy can be calculated. Two special cases, that can be determined analytically, should be pointed out:

- **Independent modes, quadratically continuously scaling**:
  if the energy of the degree of freedom distributes quadratically with the corresponding phase space coordinate $E_i \sim x_i^2$ on a continuous energy scale, the *Equipartition theorem* in section 2.2.3 can be used to determine the partition function and the average energy to $\langle E_{\text{conti}} \rangle = k_B T/2$.

- **Independent modes, equidistant discrete scaling**:
  if the energy distributes with equidistant spacing on a discrete energy scale E_n, the discrete partition function can be calculated explicitly as shown in equation (2.7) and the average energy $\langle E_{\text{disc}} \rangle$ can be calculated by equation (2.17).

3. Modeling of kinetic gases

3.1. Fokker-Planck approximation

In this thesis, the modeling of kinetic gases will focus on the approach of the kinetic Fokker-Planck ansatz. Its idea is to approximate the collision term in the Boltzmann equation (2.3) by a Fokker-Planck equation in velocity space [14]. The aim of this ansatz is to provide an approximation of the Boltzmann collision operator and a more efficient modeling. Also, restrictions due to the physical formulation like resolving collisional scales can be formulated less strict, which again reduces the computational cost of the simulations. Collisions can be considered as the change of velocities of particles. Intuitively, this happens by transferring momentum of one body to another, such as with point-like particles. A more precise look into the differential cross section in the Boltzmann collision term reveals that a modeling of intermolecular potential has to be formulated. Considering that, such a pairwise collision is just the effect of a particles surrounding potential field acting on the other particle changing each particles momentum. Instead of modeling only pairwise interaction, where one particle only acts on one other particle, the interaction effect caused by all particles in a local ensemble on all other particles can be collected in a total local field. This effectively can be expressed by a local *drift* and *diffusion* field acting to change local velocities and thus model the collisions of particles in a local ensemble. Therefore, the collision term can be approximated by the Fokker-Planck collision term by [14]

$$\left(\frac{\partial f}{\partial t}\right)_{\text{coll}} \approx \left(\frac{\partial f}{\partial t}\right)_{\text{FP}} = -\frac{\partial}{\partial v_i} A_i f + \frac{1}{2}\frac{\partial^2}{\partial v_i \partial v_j} D_{ij} f, \tag{3.1}$$

with the drift coefficient A_i and diffusion coefficient D_{ij}, which will be derived in further sections. The Fokker-Planck collision term can be translated into a coupled system of equations to determine the velocity change $\mathrm{d}v$, which is presented in section 3.2.

3.2. Modeling of the Fokker-Planck collision term

To model the dynamics of the gas, the Boltzmann equation (2.3) with the Fokker-Planck approximation (3.1) is used. To represent the stochastic particle motion, an Ito-process can be used to translate the equation into the integration scheme [8]

$$\frac{\mathrm{d}x_i}{\mathrm{d}t} = v_i, \tag{3.2}$$

$$\frac{\mathrm{d}v_i}{\mathrm{d}t} = A_i + D_{ij}\frac{\mathrm{d}W_j}{\mathrm{d}t} + F_i, \tag{3.3}$$

where $\mathrm{d}W_j$ denotes a Wiener process with zero mean and $\langle \mathrm{d}W_i \mathrm{d}W_j \rangle = \delta_{ij}$ with the Kronecker delta δ_{ij}. Particles moving according to equations (3.2) and (3.3) represent the evolution of the distribution function in the Boltzmann equation (2.3) using the Fokker-Planck collision term approximation. Their movement is determined all by the same local drift and diffusion coefficient within the same simulation cell but with an inbuilt added stochastic noise, to recover the statistical deviations. As will be presented in section 3.4, the expression for the drift contains coefficients that are made up of moments including all the particle velocities within the cell. The diffusion coefficient has a temperature dependence, that is determined by moments over all particles in the cell as well. The comparison of the Fokker-Planck collision scheme compared to the Boltzmann collision scheme is shown in figure 3.1.

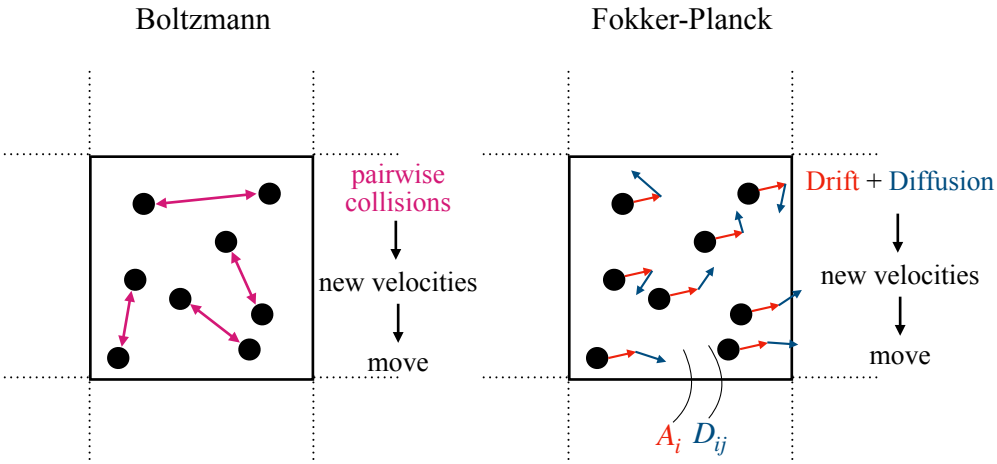

Figure 3.1.: Comparison of the Boltzmann collision and the Fokker-Planck collision scheme.

3.3. Direct Simulation Monte Carlo and Fokker-Planck

To gain the dynamics of the system, the Boltzmann equation (2.3) has to be solved by solving for the evolution of f. Due to the high dimensionality of f, a direct solution approach is too computationally expensive [7]. Therefore, the Direct Simulation Monte Carlo (DSMC) method pioneered by *Bird* [5] is used, which has been shown to be mathematically consistent with the Boltzmann equation [7]. The DSMC method discretizes the position space by a grid and approximates the state function f in velocity space by a discrete set of simulation particles. The simulation particles typically represent a large set of real molecules and statistics over their velocities give rise to macroscopic quantities.
The schematic of the DSMC algorithm is shown in figure 3.2. The algorithm can be summarized to a loop of a four step procedure: particles get generated at defined inflow boundaries and in a following step get moved according to the integration scheme. Here, the scheme is a simple *Euler* step as shown in equations (3.2). After the particles got moved, their new velocities get determined by evaluating the collisions. To model which particles are supposed to collide, the domain is divided into grid cells of the size of the mean free path, which defines the spatial scale on which collisions happen. By splitting the particle movement from the particle collision, the timestep size also needs to be smaller than the mean collision time [12]. In the original DSMC formulation by *Bird*, the Boltzmann collision operator in equation (2.4) is used, while this work will use the *Fokker-Planck* approximation for the collisions. Note that the FP collision modeling mathematically is not restricted to a cell size of the mean free path, but physically need to be chosen carefully. In DSMC, not all particles in a cell are chosen to collide. The “no time counter" (NTC) by *Bird* randomly chooses a subset of particle pairs on which collisions are performed. Finally, macroscopic quantities are calculated by collecting averages over particle properties in one grid cell.

To include the influence of internal energy states on the collision process, two models are presented in section 3.5 and 3.6. The *Master equation approach* [12] models the translational and internal energies independently. So when the collisions are calculated from translational movement, the particles post-collision velocities get

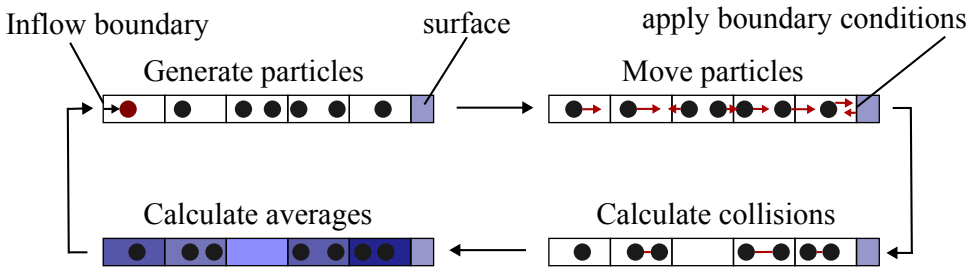

Figure 3.2.: Schematic of the DSMC algorithm adopted from [11].

adjusted by the internal energy change.
The other modeling approach is the *Direct modeling approach* [6] that includes the internal energy states in the system of equations of the production terms that determine the post-collision translational velocities directly.

3.3.1. On runtime efficiency and resolution criteria of DSMC

The main goal of the FP method is to provide an approximation of the Boltzmann collision term in equation (2.4) for computation time purposes. There are a few things that make solving the Boltzmann collision term by DSMC simulations computationally very difficult. In regions with decreasing Knudsen numbers, the number of collisions that need to be model increase strongly. Therefore, the FP model provides a method to calculate the velocity change which is independent of the Knudsen number. It calculates model coefficients for a local ensemble of particles and determines new velocities for each particle. DSMC on the other hand calculates collisions for new velocities, where the number of collisions, and therefore the number of computations, depend on the Knudsen number. This problem gets amplified by the fact, that a decreasing Knudsen number leads to a smaller mean-free path, that DSMC requires to resolve and the requirement of the timestep size to resolve the mean-collision time, which makes simulations much slower in sampling through time. While the grid refinement itself is not difficult, the number of particles in a cell obviously decreases, which makes it difficult to preserve enough information to provide good statistics. A density increasement of factor two results in half of the

mean free path. To resolve that, DSMC requires to subdivide the simulation cell into smaller cells with half the size. This splits the particles in 4 smaller grid cells for a 2D simulation and into even 8 smaller cells for a 3D simulation respectively, while there are only two times as many particles available due to the density increasement. Eventually, not enough particle remain left in the smaller cells to perform proper statistics and determine macroscopic quantities. Therefore, increasing the overall number of simulation particles in the domain can solve the problem, but will additionally increase the computation time. There are methods that deal with particle cloning to solve the latter problem but in this thesis, the FP modeling is the solution approach that is pursued. The final goal is still a hybrid coupling that uses DSMC in rarefied regions where the computation time is smaller than for the FP modeling, due to a low number of collision modeling. There, DSMC provides accurate results while FP should be used to deliver approximate results in regions where the DSMC modeling become computationally too expensive.

3.4. Cubic Fokker-Planck

To set up a model that determines the new velocities by the Fokker-Planck collision operator of section 3.1, the drift and diffusion coefficients need to be chosen. It is worth mentioning that these coefficients do not model a drift and diffusion of the position but of the velocities. The coefficients are chosen to fulfill certain properties as discussed below.
For the drift coefficient, a polynomial approach of the fluctuating vector is proposed in the literature [10] while the diffusion coefficient is build up from monatomic gases at first and further generalized in section 3.6.3 and 3.7.3. In theory, higher order polynomials can approximate the Boltzmann collision operator arbitrarily close [9]. Once the model is set up, the model parameters of the drift coefficient are chosen to fulfill transport coefficient in continuum limit by lower order Boltzmann production terms [11]. With a polynomial approximation of only linear order for the drift coefficient, a wrong Prandtl number of $Pr = 3/2$ is obtained while a quadratic model can lead to an unstable solution [10]. Therefore, a cubic ansatz is chosen which recovers the correct Prandtl number from the kinetic Gas theory of $Pr^{\mathrm{Boltz}} = 2/3$

which in terms of the linear system in equation (3.2) and (3.3) reads [10]:

$$A_i = -\frac{1}{\tau}v_i' + c_{ij}v_j' + \gamma_i(v_j'v_j' - \overline{u_j'u_j'}) + \Lambda(v_i'v_j'v_j' - \overline{u_i'u_j'u_j'}),\ i \in \{1,2,3\}, \tag{3.4}$$

where $\tau = 2\mu/p$ is a relaxation time with the dynamic viscosity μ and pressure p, the thermal velocity $\mathbf{v}' = \mathbf{V} - \mathbf{U}$ fluctuating around the bulk velocity $\mathbf{U}$ and $\mathbf{u}'$ is a realization from sample space $\mathbf{v}'$ defined as $\overline{Q(\mathbf{u}')} = \int_{\mathbb{R}^3} Q(\mathbf{v}')f\mathrm{d}\mathbf{v}'$ [10]. c_{ij} and γ_i are the model parameters that will be determined by the system of equations set up to fulfill production terms in the continuum limit [10]. Λ ensures stability and is given by [10]:

$$\Lambda = -\frac{1}{\alpha\rho^3}|\det(\pi_{ij})| \tag{3.5}$$

with the determinant $\det(\cdot)$ of the stress tensor π_{ij}, a scaling factor $\alpha = \tau(\overline{u_i'u_i'})^4$ and the mass density ρ. The model for the drift coefficient is not restricted to monatomic gases but instead generally valid for polyatomic gases. The coefficients will be determined in a way, that internal energy states are contained in the coefficients c_{ij} and γ_i. The internal states arise from the production terms and thus do not have to be enforced explicitly in the drift coefficient [6]. By comparing the relaxation of the translational heat flux with the heat flux derived by the *17-moment equation* [17], a system of equation arises, containing the internal energy states such as discussed in section 2.2.5. Further, the linear terms in (3.4) already give rise to the correct stress and energy relaxation, so all additional terms to the second order moments need to vanish [6]. The system of equations is cited in the appendix in section A.1.

The diffusion coefficient is generally given by [10] $D = \sqrt{4e_s/(3\tau)}$ but the mass specific energy $e_s = E/m$ and its weighting with correct relaxation times has to be determined correctly to cover translational and internal energy states, which is done in section 3.6.3. This is not necessary for monatomic modeling, which can make use of $E = 3k_BT/2$ directly.

3.5. Master equation approach and rate coefficients to model polyatomic gases

This section presents the Master equation approach for modeling internal energy relaxation, proposed for diatomic molecules by Hepp et al. [12] and extended to a polyatomic model by Basov et al. [4]. The calculations are performed for one

internal energy mode, which then can be applied for each arising energy mode of rotation and vibration.

Collisions in this model are considered elastic or inelastic. An elastic collision is an exchange of momentum, where only translational energy is exchanged. If the translational energy balance after a collision is not zero, it is generally called an inelastic collision and energy is transferred to some non-kinetic energy. Here, that non-kinetic part is the internal energy of the molecules that take up the energy difference. This inelastic collision terminology is kept within the master equation approach. Therefore, the collision operator is divided into an elastic and inelastic part [12]

$$\left(\frac{\partial f}{\partial t}\right)_{\text{coll}} \equiv S_{\text{coll}} = S_{\text{coll}}^{\text{el}} + S_{\text{coll}}^{\text{inel}}. \tag{3.6}$$

With the number of Z_{inel} inelastic collisions from a total of Z_{tot} total collisions, the elastic collision operator $S_{\text{coll}}^{\text{el}}$ is the fraction $Z_{\text{el}}/Z_{\text{tot}} = (Z_{\text{tot}} - Z_{\text{inel}})/Z_{\text{tot}}$ of the collision operator S_{coll}:

$$S_{\text{coll}}^{\text{el}} = \frac{Z_{\text{tot}} - Z_{\text{inel}}}{Z_{\text{tot}}} S_{\text{coll}} \approx \frac{Z_{\text{tot}} - Z_{\text{inel}}}{Z_{\text{tot}}} S_{\text{FP}}. \tag{3.7}$$

The inelastic collision operator needs to contain the modeling of a reduced translational energy exchange and a take up of internal energy. Thus, it consist of the two parts:

$$S_{\text{coll}}^{\text{inel}} = S_v + S_e \tag{3.8}$$

with the change of the number of particles in a phase space element due to an inelastic collisional particle velocity change S_v and due to a change of internal energy S_e. They are modeled as:

$$S_v \approx \frac{Z_{\text{inel}}}{Z_{\text{tot}}} \left(S_{\text{FP}} + K' \frac{\partial^2 f_n}{\partial v_i \partial v_i} \right) \tag{3.9}$$

$$S_e = \frac{Z_{\text{inel}}}{Z_{\text{tot}}} \sum_j \left(R'_{jn} f_j - R'_{nj} f_n \right) \tag{3.10}$$

where K' takes into account the energy exchange between internal and translational energy which effectively modifies the influence of the diffusion coefficient of the FP operator. A detailed derivation is shown in the appendix of [12]. R'_{jn} is the rate coefficient for the change of the internal state j to the state n in a timestep $\mathrm{d}t$. Their modeling is discussed in detail in [12].

The key idea and a strong assumption of the master equation approach is the stochastical independence of the evolution of translational velocities and internal energies:

$$f_n(\mathbf{v}, \mathbf{x}, t) = f(\mathbf{v}, \mathbf{x}, t) \cdot g_n(\mathbf{x}, t), \tag{3.11}$$

so their evolution can be modeled independently. With a common separation approach, Hepp et al. [12] can separate the equations into two individual equations resulting in:

$$\frac{\partial f}{\partial t} + v_i \frac{\partial f}{\partial x_i} = S_{\mathrm{FP}}(f) + K \frac{\partial^2 f}{\partial v_i \partial v_i} \equiv \tilde{S}_{\mathrm{FP}}(f) \tag{3.12}$$

$$\frac{\partial g_n}{\partial t} + v_i \frac{\partial g_n}{\partial x_i} = \sum_j \left(R_{jn} g_j - R_{nj} g_n \right), \tag{3.13}$$

where external forces are neglected, K and R_{jn} are substituted to $\frac{Z_{\mathrm{inel}}}{Z_{\mathrm{tot}}} K' \to K$ and $\frac{Z_{\mathrm{inel}}}{Z_{\mathrm{tot}}} R'_{jn} \to R_{jn}$, and the diffusion coefficient is summarized in $\tilde{S}_{\mathrm{FP}}(f)$ to $\tilde{D} = \sqrt{D^2 + 2K}$. For equation (3.12), the solution algorithm as set up in equations (3.2) and (3.3) can be used with the modified diffusion coefficient $\tilde{D}$ and a separate modeling of translation and internal states is possible.

Rate coefficients

For the rate coefficients R_{jn} in the master equation (3.13), three different models are suggested in [12]: the *discrete Landau-Teller* relaxation (DLT), the *continuous Landau-Teller* relaxation (CLT) and the *discrete Larsen-Borgnakke* relaxation (DLB).

DLT chooses a rate coefficient by modeling the energy levels by a quantum harmonic oscillator as in section 2.2.5 that reproduces the *Landau-Teller* relaxation for internal energies in (3.20). This results in a discrete and equidistant energy distribution $e_i = \epsilon \cdot i$ and leads to the rate coefficient that is independent of the initial state i:

$$R_{ij} \equiv R_j \equiv \frac{1}{\tau_{\mathrm{int}} \mathcal{Q}} \exp(-\beta \epsilon j). \tag{3.14}$$

CLT chooses an energy distribution on a continuous scale, where states change energy $e \to e'$ and the *Landau-Teller* relaxation in (3.20) is reproduced. The partition

function on a continuous scale reduces to $\mathcal{Q} = 1/\beta$ and the rate coefficient reads

$$R(e, e') \equiv R(e') \equiv \frac{\beta}{\tau_{\text{int}}} \exp(-\beta\epsilon'). \tag{3.15}$$

DLB distinguishes between the change of the states R_{ij} and R_{ji} to fulfill detailed balance. With the probability of P_{inel} that one collision partner changes its internal state, the VHS gas collision frequency ν_{VHS} and with a weighting function $\psi(i, j, T/\theta)$, the DLB rate coefficients are:

$$R_{ij} = \nu_{\text{VHS}}(T, n) \cdot P_{\text{inel}} \cdot \psi(i, j, T/\theta) \tag{3.16}$$

$$R_{ji} = \nu_{\text{VHS}}(T, n) \cdot P_{\text{inel}} \cdot \psi(i, j, T/\theta) \cdot \exp(-\beta(e_i - e_j)), \tag{3.17}$$

where $\psi(i, j, T/\theta)$ is a precalculated lookup table, only depending on the states i, j and the ratio of translational temperature and characteristic temperature T/θ.

3.6. Direct modeling approach for polyatomic gases

3.6.1. Generalized kinetic model

In polyatomic flows, internal excitation energies like rotation and vibration need to be considered. These internal excitations can take up a large amount of energy which on its own has an individual relaxation behaviour that needs to be modeled. The relaxation of the vibrational energy modes are slow compared to translational energy relaxation, so the vibration is generally not in thermal equilibrium with the translational energy [12]. To model the internal energies, the distribution function and the phase space have to be extended containing rotational "velocities" $\mathbf{\Omega}$ and vibrational "velocities" $\mathbf{\Xi}$:

$$f(\mathbf{v}, \mathbf{x}, t) \rightarrow f(\mathbf{v}, \mathbf{\Omega}, \mathbf{\Xi}, \mathbf{x}, t), \quad \text{define:} \quad \mathbf{\Psi} \equiv (\mathbf{v}, \mathbf{\Omega}, \mathbf{\Xi}) \in \mathcal{H}, \tag{3.18}$$

which still has to fulfill $\int_{\mathcal{H}} f \mathrm{d}\Psi = 1$. The Boltzmann equation with Fokker-Planck collision approximation generalizes to:

$$\frac{\partial f}{\partial t} + v_i \frac{\partial f}{\partial x_i} + F_i \frac{\partial f}{\partial v_i} = -\frac{\partial}{\partial \Psi_i} A_i f + \frac{1}{2} \frac{\partial^2}{\partial \Psi_i \partial \Psi_j} D_{ij} f. \tag{3.19}$$

The relaxation of the internal energies is assumed to fulfill the *Landau-Teller* relaxation:

$$\frac{\mathrm{d}E_{\mathrm{int}}}{\mathrm{d}t} = \frac{E_{\mathrm{int}}^{\mathrm{eq}} - E_{\mathrm{int}}}{\tau_{\mathrm{int}}} \tag{3.20}$$

where the total internal energy E_{int} relaxes towards the total internal equilibrium energy $E_{\mathrm{int}}^{\mathrm{eq}}$ with relaxation time $\tau_{\mathrm{int}} = Z_{\mathrm{int}}/\nu_{\mathrm{coll}}$, mean collision frequency ν_{coll} and relaxation number Z_{int}, which is a species dependent number of collisions needed to reach equilibrium [12]. Generally, there are also other models for the energy relaxation in the literature such as *Larsen-Borgnakke*, e.g. in [12], which for example recover detailed balance but are computationally more demanding. The amount of energy in the internal states varies significantly with the change in temperature. The average energies in these states are carefully derived on discrete and continuous scales in sections 3.7, while general considerations are captured in section 2.2.2.

3.6.2. Direct relaxation of translational and internal modes

The direct modeling approach extends the integration scheme of the FP approximation in equations (3.2) and (3.3) of section 3.1 by the modeling of additional internal modes. Instead of decoupling the modeling of translational and internal modes as by the master equation approach in section 3.5, the relaxation of each degree of freedom will be modeled directly. In the direct modeling approach, the states of internal energies directly influence the translational velocity change. An extension of the intergration scheme is gained from using the same integration scheme as in equation (3.2) and (3.3) with the cubic FP model in section 3.4 for the translational drift coefficient A_{tr} and the choice of linear internal drift coefficients and the resulting diffusion coefficients for the internal states:

$$\mathrm{d}v_i = -\frac{1}{\tau}v_i' + c_{ij}v_j' + \gamma_i(v_j'v_j' - \overline{u_j'u_j'}) + \Lambda(v_i'v_j'v_j' - \overline{u_i'u_j'u_j'}) + D_{\mathrm{tr}}\mathrm{d}W_i, \quad i \in \{1,2,3\} \tag{3.21}$$

$$\mathrm{d}\omega_i = -\frac{1}{2\tau_{\mathrm{rot,i}}}\omega_i\mathrm{d}t + D_{\mathrm{rot,i}}\mathrm{d}W_i, \qquad i \in \{1,...,d_{\mathrm{rot}}\} \tag{3.22}$$

$$\mathrm{d}\xi_i = -\frac{1}{2\tau_{\mathrm{vib,i}}}\xi_i\mathrm{d}t + D_{\mathrm{vib,i}}\mathrm{d}W_i, \qquad i \in \{1,...,J\}, \tag{3.23}$$

which models the change of translatinal velocities $\mathrm{d}v_i$, rotational "velocities" $\mathrm{d}\omega_i$ and vibrational "velocities" $\mathrm{d}\xi_i$. The change of position remains an *Euler*-step $\mathrm{d}x_i = v_i\mathrm{d}t$.

3.6.3. Diatomic drift and diffusion coefficients

As described in section 3.4 of the cubic FP model, the coefficients c_{ij} and γ_i in equation (3.21) are gained from matching the production terms of the Boltzmann- and FP-collision operators. Matching these terms is done using the *17-moment approximation* [17], which covers internal energy states by internal heat capacities at constant volume $c_{\mathrm{int}} = (\partial\langle E_{\mathrm{int}}\rangle/\partial T)_V$, as shown in the appendix of Gorji et al. [6]. The internal states arise from the production terms and thus do not have to be enforced explicitly in the drift coefficient [6]. Therefore, c_{ij} and γ_i directly contain the influence of the internal states by c_{int}. Also, the translational diffusion coefficient D_{tr} explicitly contains the influence of internal energy states by E_{rot} and E_{vib} as in equation (3.36).
The diffusion coefficient is generally given by [10] $D = \sqrt{4e_s/(3\tau)}$ but the mass specific energy $e_s = E/m$ and its weighting with correct relaxation times has to be determined to cover translational and internal energy states.

The assumptions for the diffusion coefficient by Gorji et al. [6] for diatomic modeling is used. Following their approach, the relaxation of each degree of freedom is modeled directly. The diffusion coefficient is assumed to be a diagonal matrix $\mathbf{D} = \delta_{ij} D_{ij}$ of the size $d \times d$, where d is the sum of translational and rotational degrees of freedom and vibrational modes. On the diagonal, the first three entries are the translational diffusion coefficients for each spatial dimension, which are assumed to be isotropic $D_{11} = D_{22} = D_{33} \equiv D_{\mathrm{tr}}^2$. The following diagonal entries are rotational and vibrational diffusion coefficients, which other than in the diatomic model are assumed to be generally not equal. Gorji et al. assume equal rotational diffusion coefficients for both two rotational degrees of freedom in their diatomic model, which is reasonable for equivalent moments of inertia in both rotational modes. In a general polyatomic molecule, this can not be assumed anymore. The set of diagonal entries results to be $(D_{\mathrm{tr}}^2, D_{\mathrm{tr}}^2, D_{\mathrm{tr}}^2, D_{\mathrm{rot},1}^2, D_{\mathrm{rot},2}^2, D_{\mathrm{rot},3}^2, D_{\mathrm{vib},1}^2, ..., D_{\mathrm{vib,J}}^2)$.
The translational and internal energies with corresponding choice of drift coefficients

are assumed as [6]

$$E_{\mathrm{tr}} = \frac{1}{2} m \overline{v_i' v_i'}, \qquad A_{\mathrm{tr,i}} = -\frac{1}{\tau_{\mathrm{tr}}} v_i', \tag{3.24}$$

$$E_{\mathrm{rot}} = \frac{1}{2} I \overline{\Omega_i^* \Omega_i^*}, \qquad A_{\mathrm{rot,i}} = -\frac{1}{2\tau_{\mathrm{rot,i}}} \Omega_i, \tag{3.25}$$

$$E_{\mathrm{vib}} = \frac{1}{2} \overline{\Xi_i^* \Xi_i^*}, \qquad A_{\mathrm{vib,i}} = -\frac{1}{2\tau_{\mathrm{vib,i}}} \Xi_i, \tag{3.26}$$

with the molecules moment of inertia I. The relaxation times are given by [6]

$$\tau_{\mathrm{tr}} = \frac{2\mu}{p}, \tag{3.27}$$

$$\tau_{\mathrm{int}} = Z_{\mathrm{int}} \tau_{\mathrm{coll}}, \tag{3.28}$$

with the species dependent collision number Z_{int} and the mean collision time [6]

$$\tau_{\mathrm{coll}} = \frac{\pi}{4} \frac{\mu}{p}. \tag{3.29}$$

The translational and rotational relaxation times are assumed to be equal for each of the modes, i.e. $\tau_{\mathrm{tr}} = \tau_{\mathrm{tr},i}$ and $\tau_{\mathrm{rot}} = \tau_{\mathrm{rot},i}$, whereas the vibrational relaxation times $\tau_{\mathrm{vib},i}$ will be modeled for each mode with individual collision numbers $Z_{\mathrm{vib},i}$.
For the diatomic case, Gorji et al. [6] derived an expression for the internal diffusion coefficients. Multiplying the FP equation (3.6.1) with an internal energy, E_{rot} and E_{vib} respectively, an expression for the energy change in time can be gained. Comparing the result with the *Landau-Teller* relaxation in equation (3.20), the internal diffusion coefficients $D_{\mathrm{rot}} = \sqrt{2E_{\mathrm{rot}}^{\mathrm{eq}}/(I\tau_{\mathrm{rot}})}$ and $D_{\mathrm{vib}} = \sqrt{2E_{\mathrm{vib}}^{\mathrm{eq}}/(\tau_{\mathrm{vib}})}$ are derived. A detailed derivation of internal diffusion coefficients D_{int} has been carried out and is shown in the appendix in section A.2.
A translational diffusion coefficient D_{tr} has been proposed by Gorji et al. [6] by

$$D_{\mathrm{tr}} = \sqrt{\frac{2}{3m}(\alpha_{\mathrm{tr}} E_{\mathrm{tr}} + \alpha_{\mathrm{rot}} E_{\mathrm{rot}} + \alpha_{\mathrm{vib}} E_{\mathrm{vib}})}, \tag{3.30}$$

with the weights $\alpha_{\mathrm{tr}} = 2/\tau_{\mathrm{tr}} - 2/(3\tau_{\mathrm{rot}}) - 2\mathcal{Z}/(3\tau_{\mathrm{vib}})$, $\alpha_{\mathrm{rot}} = 1/\tau_{\mathrm{rot}}$, $\alpha_{\mathrm{vib}} = \mathcal{Z}/\tau_{\mathrm{vib}}$ with $\mathcal{Z} = E_{\mathrm{vib}}^{\mathrm{eq}}/(k_B T)$.

3.7. Extension of the direct modeling approach to polyatomic gas

3.7.1. Translational, rotational and vibrational energy assumptions

In the presented model, the internal energies of a molecule are treated differently depending on whether or not the energies are modeled continuous or discrete. Translational and rotational energy levels are assumed to be distributed on a continuous scale and are defined as in equation (3.24) and (3.25). The rotational energy is given by $E_{\text{rot}} = \frac{1}{2} I\omega^2$ with its rotation frequency ω and the molecular shape dependent moment of inertia I [2]. Vibrational energy states on the other hand are considered on a discrete scale and are assumed to follow the dynamics of a quantum harmonic oscillator. Thus, the spacing of the energy levels is equidistant [2] and the discrete vibrational energy states can be evaluated by using $E_{\text{int,n}} = nk_B\theta_{\text{int}}$, measured from the zero point energy [2], with the characteristic vibrational temperature θ_{vib} used to calculate the n'th vibrational energy state.
This assumption of a harmonic potential should show deviations in theoretical prediction to experimental measurements. However, the advantage of using a harmonic potential is that the sum in the partition function can be evaluated analytically and therefore allows for efficient calculation. The total energy E_{tot} is defined as the sum of the translational energy E_{tr} and internal energies E_{int}, where internal energies will be determined by rotation and vibration of the molecules only

$$E_{\text{tot}} = E_{\text{tr}} + E_{\text{int}} = E_{\text{tr}} + E_{\text{rot}} + E_{\text{vib}}, \tag{3.31}$$

hence we will neglect electron excitement energies. Electron excitement energies may change not only by collisions but generally spontaneously. Therefore a different model approach is necessary and not covered within the approach presented in this work.

3.7.2. Polyatomic internal energies

Considering a specific energy on a continuous scale that depends on d of the total number of d_{tot} degrees of freedom, the dependencies read $E = E(x_1, ..., x_d)$, where the x_i are arbitrary variables whose change contribute to a change of E. We further

assume that each degree of freedom contributes independently of all other degrees of freedom to the total energy and the energy can be written as the sum of the individual energies $E_i = E_i(x_i)$ as $E = \sum_{i=1}^{d} E_i(x_i)$. If we can further assume that the energy scales quadratically with x_i (assume $E_i \sim cx_i^2$), such as for the rotational energy $E_{\text{rot}} \sim \omega^2$, the average energy $\langle E \rangle_i$ per degree of freedom can be determined[3] to $\langle E \rangle_i = k_B T/2$. Determining the correct degrees of rotational freedom d_{rot} give rise to the rotational energy:

$$\langle E_{\text{rot}} \rangle = \frac{d_{\text{rot}}}{2} k_B T. \tag{3.32}$$

The result is independent of the moment of inertia and thus of the molecular construction. For the vibrational energy, the considered equidistant discrete energy levels have multiple vibrational modes in a polyatomic molecule simultaneously. For a molecule consisting of N atoms, the number of vibrational modes[2] are $\tilde{J} = 3N - 5$ for linear molecules and $\tilde{J} = 3N - 6$ for non-linear molecules. For degenerate modes, fewer number of modes J can be modeled when covering its multiple occurrence by the degeneracy factor g_j. Assuming that each vibrational mode is independent and therefore contributes to the overall vibrational energy independently, the partition function is the product of each individual partition function of mode j, while raising to the power of degeneracy g_j of the j'th mode[2]. Therefore the average internal vibrational energy results in

$$\langle E_{\text{vib}} \rangle = k_B \sum_{j=1}^{J} \frac{g_j \cdot \theta_{\text{vib},j}}{\exp(\theta_{\text{vib},j}/T_{\text{vib},j}) - 1}. \tag{3.33}$$

3.7.3. Polyatomic drift and diffusion of internal and translational energy

The drift introduced with the generalized kinetic model in section 3.6.1 already contains the influence of polyatomic energies in the system of equations arising from the production terms. However, the diatomic expression for the diffusion coefficient by Gorji et al.[6] has to be generalized. This is done with the assumptions of independent modes and the total energy as the sum of all individual energies. This decoupling of the internal modes lead to a *Landau-Teller* relaxation of each mode in the total sum, resulting in a diffusion coefficient for each degree of freedom. To derive the internal diffusion coefficients, an analytic derivation for each mode is

carried out and shown in detail in the appendix A.2. The thermal equilibrium energy of rotational energy on a continuous scale is given by the equipartition theorem and determines $k_B T/2$ per rotational degree of freedom. The thermal equilibrium energy of each vibrational mode on a discrete energy scale is given by equation (3.33) for $J = 1$. Keeping in mind the different continuous and discrete energy assumptions from section 3.7.1 when determining the equilibrium energy for the *Landau-Teller* comparison, the internal diffusion coefficients generalize to

$$D_{\mathrm{rot,i}} = \sqrt{\frac{k_B T}{I_i \tau_{\mathrm{rot}}}}, \qquad i \in \{1, ..., d_{\mathrm{rot}}\}, \tag{3.34}$$

$$D_{\mathrm{vib,i}} = \sqrt{\frac{2}{\tau_{\mathrm{vib,i}}} \frac{\theta_{\mathrm{vib},i}/T}{(\exp(\theta_{\mathrm{vib},i}/T) - 1)}}, \quad i \in \{1, ..., J\}, \tag{3.35}$$

where I_i are the three generally different moments of inertia of the molecule around its three rotation axes and $\theta_{\mathrm{vib},i}$ is the vibrational temperature of the i'th vibrational mode. The vibrational relaxation times might be modeled with equal values for equal atomic bonds.

A translational diffusion coefficient D_{tr} has been proposed by Gorji et al. [6] and will be extended to cover the influence of multiple vibrational modes by substituting $\alpha_{\mathrm{vib}} E_{\mathrm{vib}} \to \sum_i^J \alpha_{\mathrm{vib},i} E_{\mathrm{vib},i}$

$$D_{\mathrm{tr}} = \sqrt{\frac{2}{3m}(\alpha_{\mathrm{tr}} E_{\mathrm{tr}} + \alpha_{\mathrm{rot}} E_{\mathrm{rot}} + \sum_{i=1}^{J} \alpha_{\mathrm{vib},i} E_{\mathrm{vib},i})}, \tag{3.36}$$

with the generalized weights $\alpha_{\mathrm{tr}} = 2/\tau_{\mathrm{tr}} - d_{\mathrm{rot}}/(3\tau_{\mathrm{rot}}) - \sum_i^J \mathcal{Z}_{\mathrm{vib},i}/(3\tau_{\mathrm{vib},i})$, $\alpha_{\mathrm{rot}} = 1/\tau_{\mathrm{rot}}$, $\alpha_{\mathrm{vib},i} = \mathcal{Z}_{\mathrm{vib},i}/\tau_{\mathrm{vib},i}$ with $\mathcal{Z}_{\mathrm{vib},i} = g_i E^{\mathrm{eq}}_{\mathrm{vib},i}/(k_B T/2)$.

3.8. Energy conservation

The way the direct modeling method is formulated in section 3.6.2, it adds an independent stochastic noise on each degree of freedom. This recovers the natural stochastic fluctuation on each energy state of the degree of freedom and will add up to a fluctuation in the total energy. With this fluctuation, the total energy is conserved on average, but not locally in time. And instead of compensating an energy drop in translation by increasing internal energies, the internal states will follow the fluctuation of the translation. Physically, the opposite is desired, and an

exact energy conservation is needed.
To build energy conservation that still recovers the dynamics of the modeling method, the change of translational energies will be determined as formulated by the direct modeling method, but rescaled depending on the change of the internal energy states. This scaling factor α is derived by following the idea of Hepp et al. [11]. The goal is to scale the updated thermal velocities in timestep $n+1$, i.e. $v'^{n+1} \rightarrow \alpha v'^{n+1}$, such that they preserve energy after the internal states have already been updated from timestep $n \rightarrow n+1$

$$\frac{1}{2}m_i(\alpha v'^{n+1}_i)^2 + E^{n+1}_{\text{rot}} + E^{n+1}_{\text{vib}} = \frac{1}{2}m_i(v'^{n}_i)^2 + E^{n}_{\text{rot}} + E^{n}_{\text{vib}}, \tag{3.37}$$

which leads to the scaling factor

$$\alpha = \sqrt{\frac{\frac{1}{2}m_i(\alpha v'^{n+1}_i)^2 + E^{n+1}_{\text{rot}} + E^{n+1}_{\text{vib}} - E^{n}_{\text{rot}} - E^{n}_{\text{vib}}}{\frac{1}{2}m_i(v'^{n+1}_i)^2}}. \tag{3.38}$$

With the energy conservation guaranteed by the scaling factor, even large timestep sizes can be applied [12].

3.9. Numerical modeling

3.9.1. Integration scheme

To update the position, translational velocities and internal states, an intergration scheme to solve the equations of motion (3.3) and (3.2) has to be derived. The model uses the drift and diffusion coefficients as derived in previous sections. To integrate the velocity changes, the drift term is separated into a linear part, that will be integrated analytically and a non-linear part, that will be integrated by an *Euler* step, following the derivation by Hepp et al. [12] and neglecting external forces F_i, the velocity update reads

$$\begin{aligned} v^{n+1}_i = \frac{1}{\alpha}\Bigg[& v'^{n}_i \exp\left(-\frac{\Delta t}{\tau_{\text{tr}}}\right) + \left(1 - \exp\left(-\frac{\Delta t}{\tau_{\text{tr}}}\right)\right)\tau_{\text{tr}} N^n_i \\ & + W_i \sqrt{\frac{D^2_{\text{tr}}}{2}\tau_{\text{tr}}\left(1 - \exp\left(-2\frac{\Delta t}{\tau_{\text{tr}}}\right)\right)}\Bigg] + v^n_i - v'^{n}_i, \end{aligned} \tag{3.39}$$

which updates the thermal velocity $\mathbf{v}' = \mathbf{v} - \mathbf{u}$, where $\mathbf{u}$ is the bulk velocity, W_i are independent standard normal variates and N_i^n is the non-linear term

$$N_i^n = c_{ij}v_j' + \gamma_i(v_j'v_j' - \overline{v_j'v_j'}) + \Lambda(v_i'v_j'v_j' - \overline{v_i'v_j'v_j'}), \tag{3.40}$$

with the energy conservation scaling factor α from section 3.8. To calculate the velocity update, the system of equation as shown in the appendix A.1 has to be solved in each timestep to determine the coefficients c_{ij} and γ_i.
Although both methods, the master equation approach in section 3.5 and the direct modeling approach 3.6, integrate the same equations of motion, the translational velocity update still differs by the different diffusion coefficients D.
The integration of each internal degree of freedom by the direct modeling approach can be integrated analytically, as has been shown by Gorji et al. [6]. For the rotational and vibrational relaxation, the following intergration scheme is adopted:

$$\omega_i^{n+1} = \omega_i^n \exp(-\Delta t/2\tau_{\text{rot}}) + D_{\text{rot},i}\sqrt{\tau_{\text{rot}}(1 - \exp(-\Delta t/\tau_{\text{rot}}))}W_{\text{rot},i}, \tag{3.41}$$

$$\xi_i^{n+1} = \xi_i^n \exp(-\Delta t/2\tau_{\text{vib},i}) + D_{\text{vib},i}\sqrt{\tau_{\text{vib},i}(1 - \exp(-\Delta t/\tau_{\text{vib},i}))}W_{\text{vib},i}. \tag{3.42}$$

This way, the polyatomic direct modeling method differs from the master equation approach in explicitly relaxing each internal degree of freedom by an integration scheme via an *Euler* step, whereas the master equation approach models an energy exchange between internal and translational modes by directly generating energy levels via rate coefficients.

3.9.2. Numerical routine

Translating the modeling and its integration schemes of equations (3.39), (3.41) and (3.42) into code has been done as listed by the pseudocode routine in section A.3 of the appendix. Within this Master's thesis, the Fokker-Planck algorithm has been implemented into the DSMC SPARTA code [20] following the structure of algorithm 1 in the appendix.

4. Verification and code-to-code comparison

To verify and validate the polyatomic direct Fokker-Planck model as a working approximation of the collision operator, the model has been implemented and several test cases are studied. With the focus on polyatomic modeling, the energy distribution and temporal relaxation of their multiple internal degrees of freedom are investigated in detail. The tests include comparison with analytical results if possible and comparison with the different validated models and validated reference data. Test cases will be performed using the species N_2, CO_2 and CH_4 using the variable-hard-sphere (VHS) collision model and parameters as shown in table 4.1.
The direct model has been implemented into the open source DSMC solver SPARTA [20] and comparisons will be done with analytic results if possible, with DSMC results using SPARTA, a FP-master equation implementation from section 3.5, that has been implemented into SPARTA as well, and with reference date by the polyatomic Fokker-Planck model of Pfeiffer et al. that use the PICLas code of the University of Stuttgart [19].
The test cases will increase in complexity, i.e. starting with heat bath simulations that will simulate particles in a box, that are initialized with different temperatures for translation, rotation and vibration. Therefore, by definition their corresponding energies are not in equilibrium. With temporal integration of the system, the relaxation of the different energies and temperatures are observed. The heat bath simulations will be investigated for diatomic and polyatomic species. The diatomic test case uses molecular nitrogen N_2, while two different polyatomic test cases are performed using CO_2 to include investigations covering linear polyatomic molecules and a test case with CH_4 as an irregular polyatomic molecule including the testing with degenerate vibrational modes. The results will take a look at temperature and energy plots and are compared with reference data from SPARTA [20] and Pfeiffer et al. [19].

Table 4.1.: VHS parameters of N_2, CO_2 and CH_4 as given by SPARTA [20] and Pfeiffer et al. [19]

Ref.		vib. temp. θ_{vib} / K (degeneracy)	ω_{VHS}	T_{ref} / K	d_{ref} / m
[20]	N_2	3371.0	0.74	273	4.07×10^{-10}
[19]	CO_2	1918.6, 3382.0, 959.7(2)	0.8	273	5.62×10^{-10}
[19]	CH_4	4194.9, 2206.0(2), 4341.6(3), 1878.1(3)	0.7	298	3.64×10^{-10}

In a second set of test cases, the model is tested to be capable of recovering full flow field structures by hypersonic simulations around an object. 2D simulations of hypersonic flow around a cylinder will be performed and the flow field will be investigated, looking at the particle density field and temperature field. The accuracy of peak values and spacial deviations will be compared with the DSMC and FP-master equation methods for diatomic and polyatomic species in flow field and line plots. Beyond the validation of the model, the computational efficiency for decreasing particle densities and comparisons of the computation time with DSMC and with the master equation approach of the Fokker-Planck modeling are shown in last section.

4.1. Relaxation of energies and temperatures

4.1.1. Simulation setups

The relaxation tests are separated into diatomic tests in section 4.1.2 comparing the relaxation of the FP-direct model with SPARTA DSMC [20] and polyatomic tests in section 4.1.3 comparing the relaxation of the FP-direct model with the FP model by Pfeiffer et al. from their PICLas code [19]. The test cases are performed using the variable-hard-sphere (VHS) model for particle collisions with parameters as shown in table 4.1 for the different species. Note that for better visualization purposes, not every data point from every timestep is marked in the plots, but instead only points of every few timesteps. This does not mean that the points are average values but really only a subset of the whole data to have a cleaner visualization.

In previously presented results at the Aerospace Europe Conference 2023 by Nagel et al. [18], the relaxation of the model has been validated predicting correct limits but with fluctuations in total energies, due to a previous version that did not include the scaling factor α from equation (3.38) to recover exact energy conservation. This was consistent with the formulation of the model and the results showed the expected

behaviour, especially in terms of the overall energy fluctuation. The energy is then only conserved on average and fluctuations in the total energy again influence the direction of the change of all degrees of freedom all in the same direction, due to the provided overall total energy and therefore the aimed limit of each degree of freedom. With the improvement of the scaling factor, the translational and internal energies show contrary fluctuations to exactly match the energy exchange and conserve energy, which is required by a physically accurate description.

4.1.2. Diatomic relaxation tests

The relaxation tests of translational and internal energies and temperatures for diatomic species using N_2 are shown in figures 4.1 and 4.2, comparing the FP-direct model with a DSMC reference solution using SPARTA. The test simulates a box of volume $V = (1\ \mathrm{m})^3$ at a particle density of $n = 10^{20}\ \mathrm{m}^{-3}$, using 10 000 simulation particles that are initialized with temperatures of $T_{\mathrm{tr}} = 9000$ K, $T_{\mathrm{rot}} = 3000$ K and $T_{\mathrm{vib}} = 4000$ K. To resolve the mean collision time τ_{coll} as required by the DSMC reference method, a timestep of $\Delta t = 10^{-6}$ s is used for both methods. For simplicity, the collision relaxation numbers are chosen to be $Z_{\mathrm{rot}} = 5$ and $Z_{\mathrm{vib}} = 10$. The VHS collision model parameters and characteristic vibrational temperatures are listed in table 4.1.

The results are in very good agreement with the DSMC reference data. The FP direct model shows small temporal deviations of translation and rotation compared to the DSMC predictions of SPARTA, but fits the limits very well. Due to the temporal deviations of the translational and rotational energies, the theoretical expectations of the *Landau-Teller* relaxation in equation (B.3) is used to calculate theoretical predictions for a translational and rotational energy exchange. The results are plotted in figure 4.3 and show, that the FP direct model matches the demanded *Landau-Teller* relaxation very accurately.

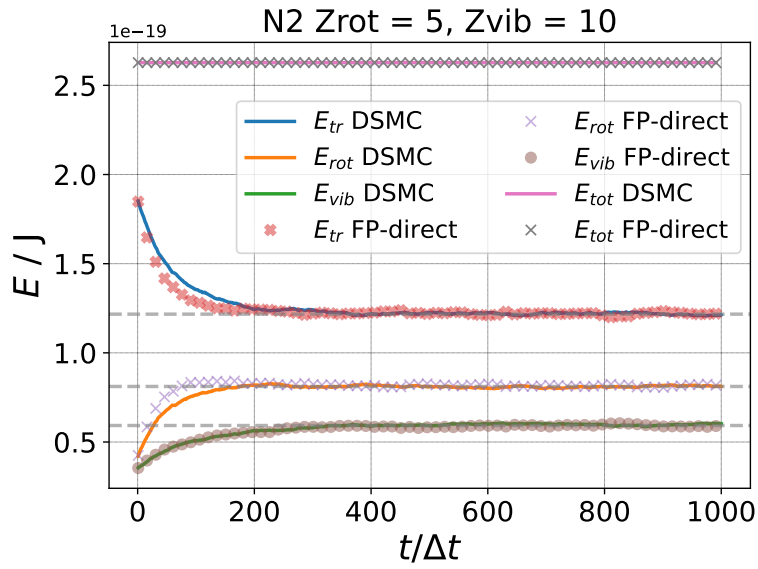

Figure 4.1.: Relaxation of translational, rotational and vibrational energy initialized at non-equilibrium temperature for N_2.

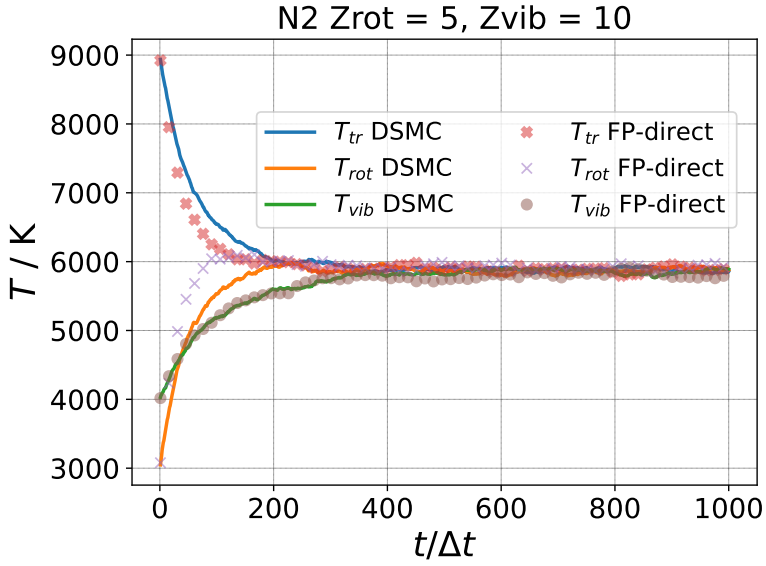

Figure 4.2.: Relaxation of translational, rotational and vibrational temperature initialized at non-equilibrium temperature for N_2.

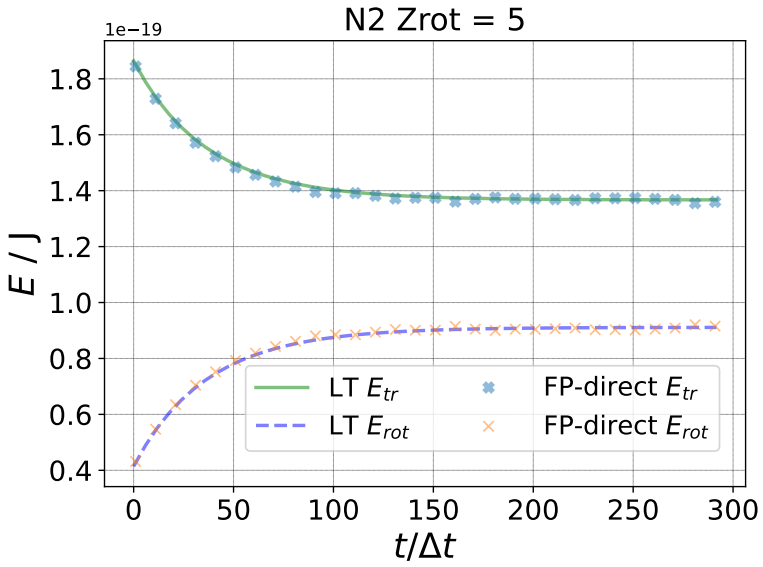

Figure 4.3.: Relaxation of translational and rotational energies comparing the FP direct model with the *Landau-Teller* (LT) relaxation of equation (B.3) for N_2.

4.1.3. Polyatomic relaxation tests

The relaxation tests of translational and internal energies and temperatures for polyatomic species are investigated for CO_2 and CH_4 and are shown in figures 4.4 and 4.5. The plots show the results of the polyatomic FP-direct model with the reference data from the polyatomic FP-model using PICLas of Pfeiffer et al. [19]. The volume of the heat bath simulation box is chosen as in the reference to $V = (4.6 \times 10^{-4})^3 \mathrm{m}^3$, also using 200 000 simulation particles. A particle number density of $n = 2 \times 10^{22} \mathrm{m}^{-3}$ is simulated with initialized temperatures of $T_{\mathrm{tr}} = 10000$ K, $T_{\mathrm{rot}} = 7500$ K and $T_{\mathrm{vib}} = 5000$ K. The timestep size is set to $\Delta t = 10^{-8}$ s and 600 timesteps are simulated. The VHS collision model parameters and characteristic vibrational temperatures are again listed in table 4.1 and the relaxation numbers are chosen to be $Z_{\mathrm{rot}} = 10$ and $Z_{\mathrm{vib}} = 50$.
The results in figures 4.4 and 4.5 show that the polyatomic FP direct extension is in very accurate agreement with the reference data of Pfeiffer et al., predicting the correct temporal relaxation into the equilibrium.

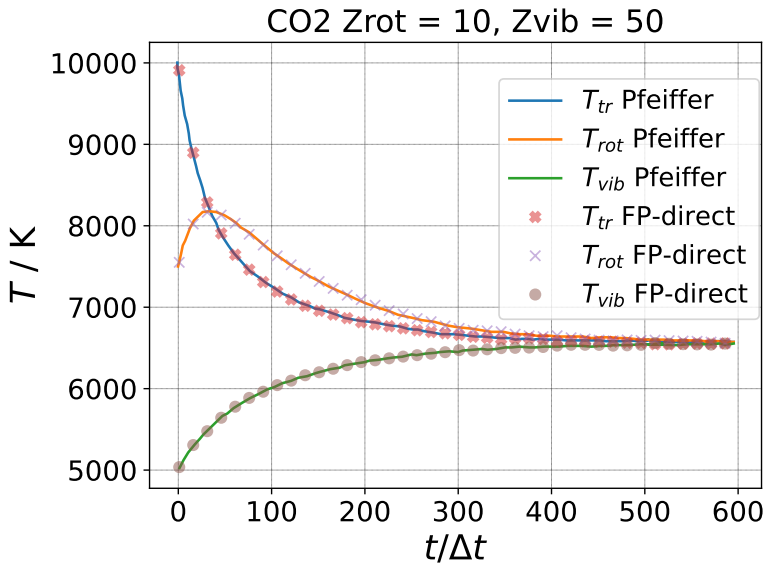

Figure 4.4.: Relaxation of translational, rotational and vibrational temperature initialized at non-equilibrium temperature for CO_2.

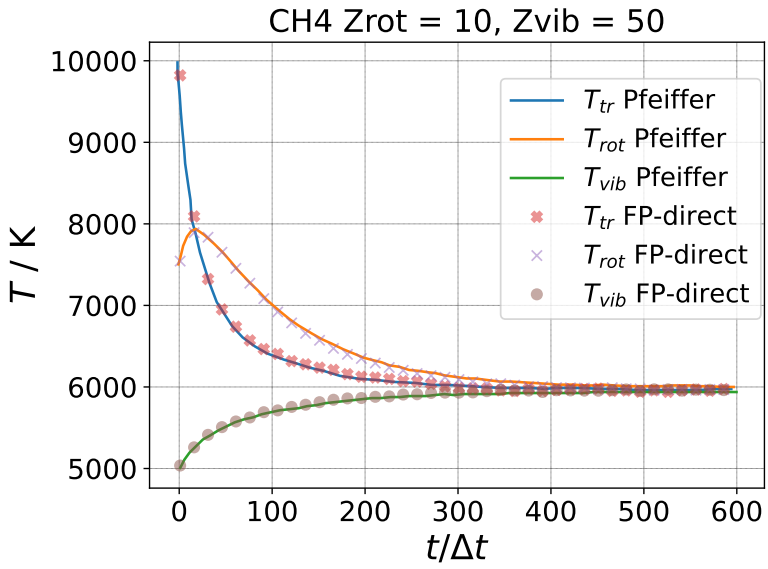

Figure 4.5.: Relaxation of translational, rotational and vibrational temperature initialized at non-equilibrium temperature for CH_4.

4.2. 2D hypersonic flow around a cylinder

4.2.1. Simulation setup

The second set of test cases take a look at the well known flow field of a hypersonic flow around a cylinder. The tests will be separated into diatomic and polyatomic cases as in the relaxation tests, and use the DSMC implementation in SPARTA [20] for the diatomic reference data and the polyatomic FP-master equation implementation [4] for the polyatomic reference. The VHS collision model is used and the model parameters are shown in table 4.1.

The goal of the Fokker-Planck collision approximation by equation (3.1) is to have a computationally more efficient collision modeling than DSMC at lower Knudsen numbers. Therefore, the 2D flow test is performed in the lower range of the transition flow regime as characterized by figure 2.1. The runtime efficiency for varying Knudsen numbers is then analyzed in a separate step in section 4.3. For the test of the 2D hypdersonic flow field around a cylinder of length $L = 1$ m, a Knudsen number of $Kn = 0.25$ at a Mach number of $Ma = 10$ is chosen and the inflow particle temperatures are equal to the wall temperature of the cylinder $T_\infty = T_\mathrm{w}$. This means that the translational velocity corresponds to a velocity from $Ma = 10$ with an added thermal velocity to the corresponding thermal temperature $v_\mathrm{tr} = v_{Ma} + v'_\mathrm{th}(T_\infty)$. The simulations make use of the symmetry and simulate only one of the symmetry halves. To gain comparable results, the DSMC simulations are performed first, with the necessary grid and timestep size refinements as demanded by the DSMC resolution criteria in section 3.3 and the same grid and adjusted timestep size is used for the followed investigated FP-direct simulations, even though these restrictions do not necessarily account for the FP model.
The results discussed in subsequent sections show the flow fields of the particle number density and the temperature fields, where the convention of the flow always entering from the left boundary is used, streaming through the domain from left-to-right. The reference solution is always displayed at the top and the FP modeling at the bottom of the figures. Further, these investigated quantities are plotted downstream through the stagnation point, to investigate peak values and spacial deviations.

4.2.2. Diatomic 2D flow around a cylinder

The results of the flow field and lineplot data for the diatomic 2D flow around a cylinder are shown in figures 4.6 to 4.9, comparing the particle number density and the thermal temperature gained from the DSMC solution and the FP-direct modeling. Further details are shown in figures 4.10 and 4.11 with lineplots of the translational and rotational energies separately. With a chosen free stream temperature of $T_\infty = 300$ K, vibrational energy is not excited for the N_2 tests.
The flow field of the particle number density in figure 4.6 shows only small deviations and recovers the density distribution of the shock structure very well. The flow seems to reach a little bit further around the cylinder and into the wake region. The corresponding lineplot in figure 4.8 shows very good agreement of the two methods, while the FP-direct model slightly overestimates the maximum density increasement in the stagnation point and close to the cylinder in the wake. The thermal temperature field in figure 4.7 shows larger spacial deviations of the FP-direct model compared to DSMC, overestimating the shock thickness and predicting the location of the maximum temperature a little bit closer to the stagnation point. This also can be seen in the corresponding lineplot in figure 4.9, showing that the FP-direct temperature curve starts to increase with decreasing distance to the stagnation point earlier than the DSMC curve. In the wake region behind the cylinder, also minor spacial difference occur by the FP-direct model compared to the DSMC results. However, besides these spacial deviations, the maximum values of the thermal temperature are estimated very well by the FP-direct modeling in comparison with the DSMC results. A study worth mentioning at this point has been done by Lofthouse et al. in 2008 [15], comparing DSMC with CFD also using a flow around a cylinder at $Kn = 0.25$ and $Ma = 10$. In their study they did not use equal free stream and wall temperatures and did not focus on internal degrees of freedom, using Argon as species. In their results, the shock thickness of the CFD results is smaller than the DSMC results but the temperature maximum of the CFD simulation is also closer to the body than for the DSMC result. This is consistent with the expectation due to a matching of the FP production terms with the continuum limit. Their results are shown in the appendix in section B.2.

A detailed look into thermal and internal temperatures reveals that the distribution does not quite match the expectations by the reference. In equilibrium regions in the flow field, the distribution of the energies match the expectations well, as validated

by the relaxation tests. Deviations occur in the shock regions, where the flow is in high non-equilibrium and also in the wake region, where a low particle number may effect the results lager statistical deviations. This leads to a slightly overestimated rotational energy in these regions but approaches the reference solution again further downstream in the wake.

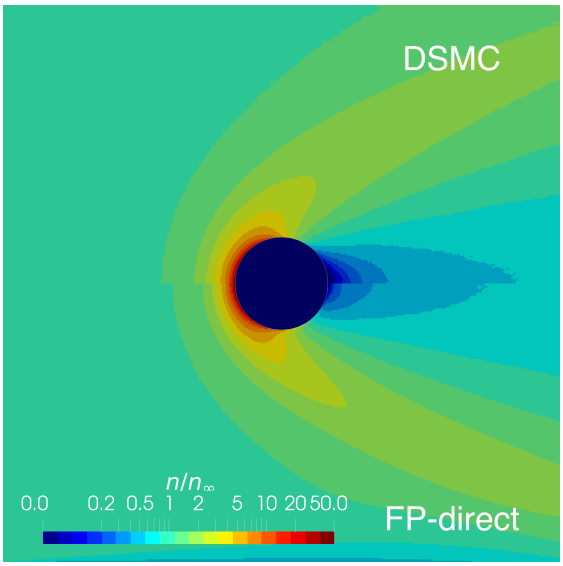

Figure 4.6.: N_2 particle density field of a 2D flow around a cylinder using DSMC (top) and the FP-direct model (bottom) at $Kn = 0.25$ and $Ma = 10$.

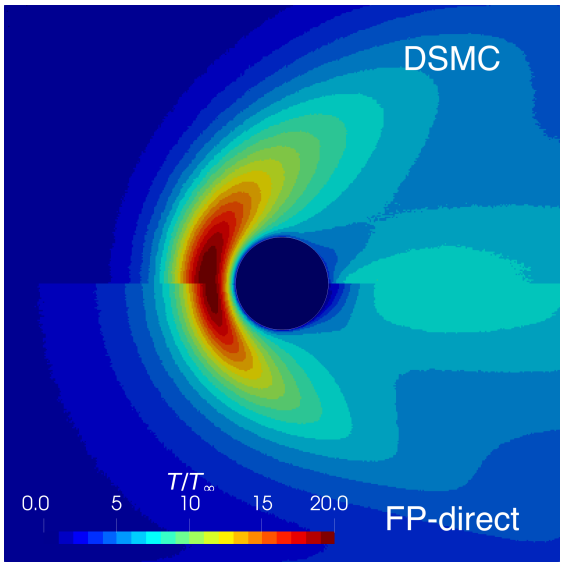

Figure 4.7.: N_2 temperature field of a 2D flow around a cylinder using DSMC (top) and the FP-direct model (bottom) at $Kn = 0.25$ and $Ma = 10$ with $T_\infty = T_{\text{wall}}$.

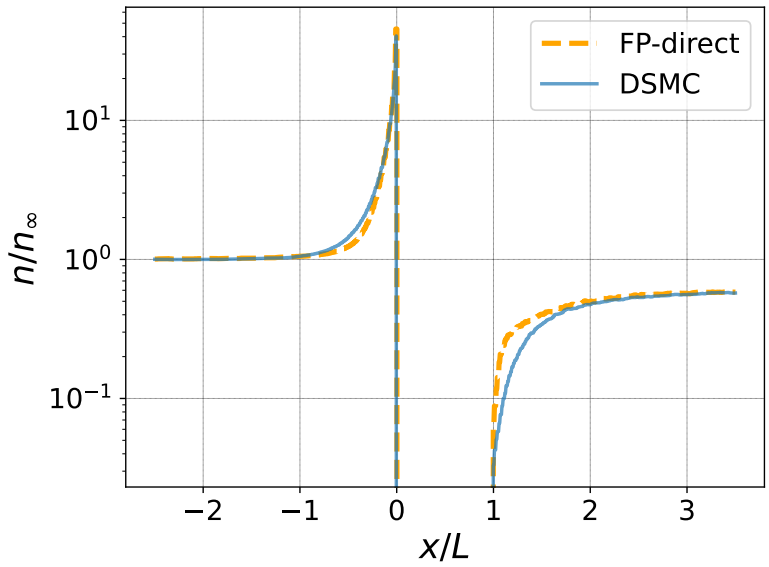

Figure 4.8.: Normalized particle density plot of the flow field downstream through the stagnation point in figure 4.6, normalized by characteristic length given by the cylinder diameter L for N_2.

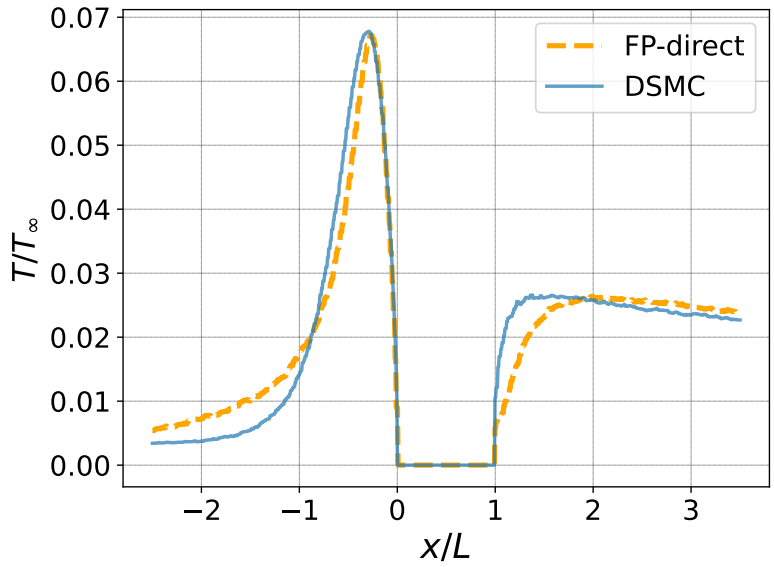

Figure 4.9.: Normalized temperature plot of the flow field downstream through the stagnation point in figure 4.7, normalized by characteristic length given by the cylinder diameter L for N_2.

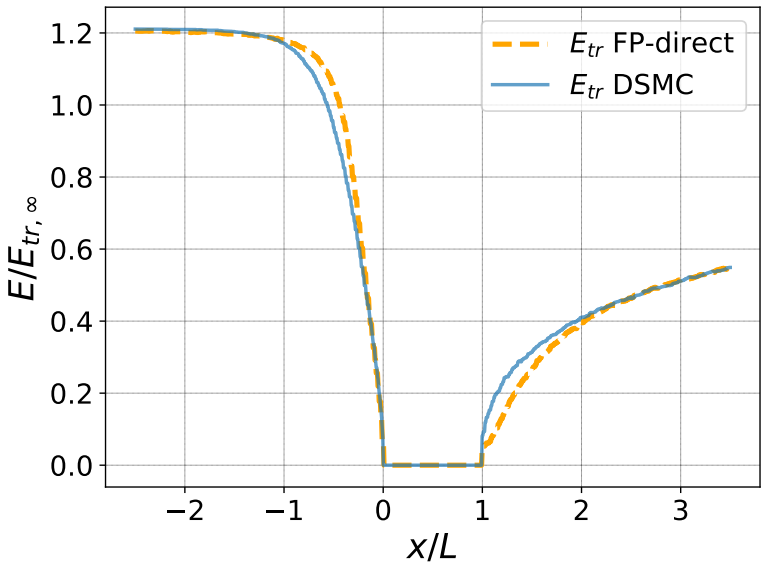

Figure 4.10.: Normalized translational energy plot of the flow field downstream through the stagnation point in figure 4.7, normalized by characteristic length given by the cylinder diameter L for N_2.

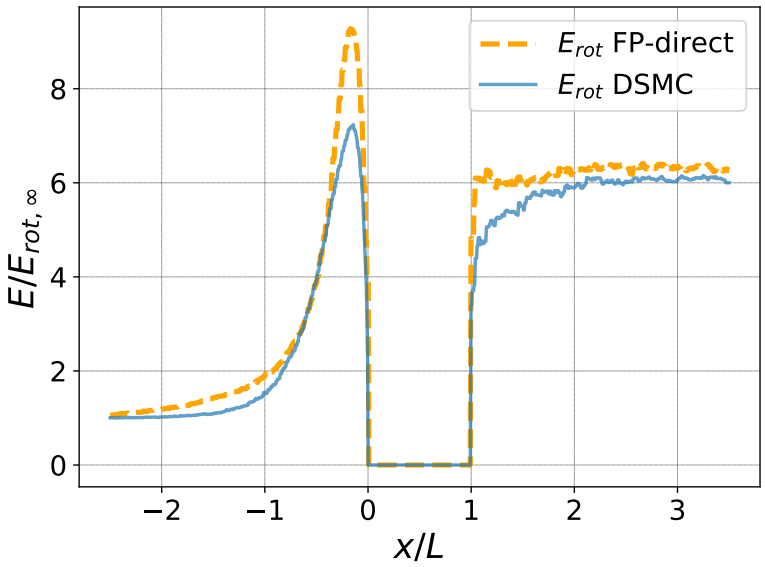

Figure 4.11.: Normalized rotational energy plot of the flow field downstream through the stagnation point in figure 4.7, normalized by characteristic length given by the cylinder diameter L for N_2.

4.2.3. Polyatomic 2D flow around a cylinder

The results of the flow field and lineplot data for the polyatomic 2D flow around a cylinder are shown in figures 4.12 to 4.18, comparing the particle number density and the thermal temperature gained from the DSMC solution and the FP-direct modeling for CO_2, as well as the translational and internal energy along the symmetry line.
The results of the polyatomic particle number density shown in figure 4.12 are in good agreement with the reference case. Small deviations can be seen in the wake region, which predicts a smaller rarefied region in the flow field. In contrast to the diatomic results, the peak value of the polyatomic particle number density in the stagnation point in figure 4.14 are estimated very accurately, which is not surprising, as both compared methods use the FP approximation. Besides a spacial shift of the density increasement in the wake region, the overall lineplot curves of the reference and the FP-direct model match well.
The results of the polyatomic thermal temperature field in figure 4.13 shows regions of good agreement and regions of larger deviations. The temperature field in the free stream flow all the way downstream to the stagnation point and the surrounding overall shock structure is recovered quite well. However, deviations in the temperature field can be observed in the wake region.
The lineplot of the thermal temperature in figure 4.15 confirms the observation in the temperature flow field. The temperature plot shows good agreement in front of the cylinder through the shock to the stagnation point with only small spacial deviations. Larger deviations of the temperature field occur in the wake region.
Taking a look at the lineplots in figures 4.15, 4.17 and 4.18 show that all three plots show overall good agreement with the reference, but deviations are observed for the rotational and vibrational energies in the wake region. This observation is consistent with the overestimation of the temperature in the wake.
Careful reassurance of the correct vibrational energy has been done, including investigations on the degeneracy of CO_2. As listed in table 4.1, CO_2 has 4 modes, two of which are degenerate. To make sure that the correct degeneracy is included, two simulations have been compared, one performing 3 modes and counting the degenerate modes twice in the total energy and another one performing 4 modes, two of which have the same vibrational excitation energy defined by the vibrational temperature θ_{vib}. Both simulation showed the same deviations of vibrational energy.

In the 2D tests, the overall structures and energy values are predicted well and deviations occur in rarfied regions, where internal energies are slightly overestimated. The FP direct model appears to be more sensitive to deviations in rarefied regions than the FP master approach.

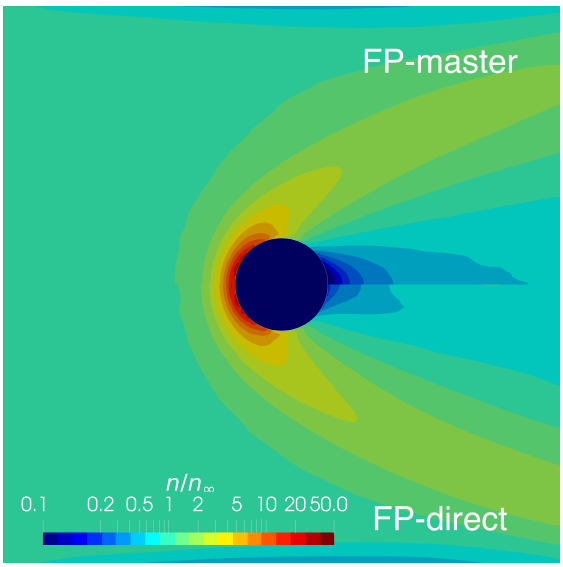

Figure 4.12.: CO_2 particle density field of a 2D flow around a cylinder using the FP-master (top) and the FP-direct model (bottom) at $Kn = 0.25$ and $Ma = 10$.

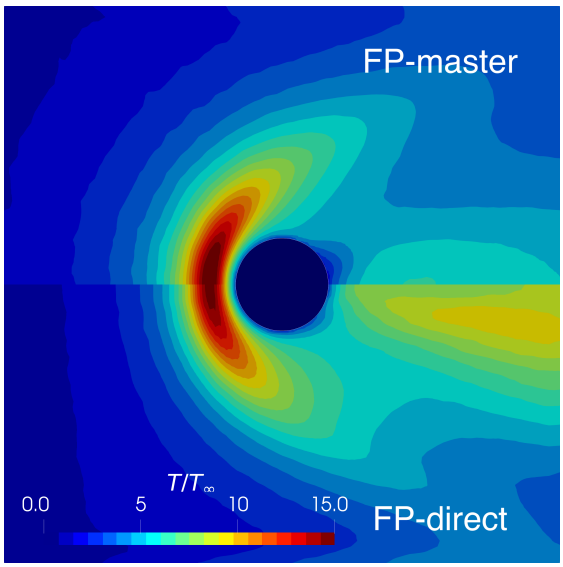

Figure 4.13.: CO_2 temperature field of a 2D flow around a cylinder using the FP-master (top) and the FP-direct model (bottom) at $Kn = 0.25$ and $Ma = 10$ with $T_\infty = T_{\text{wall}}$.

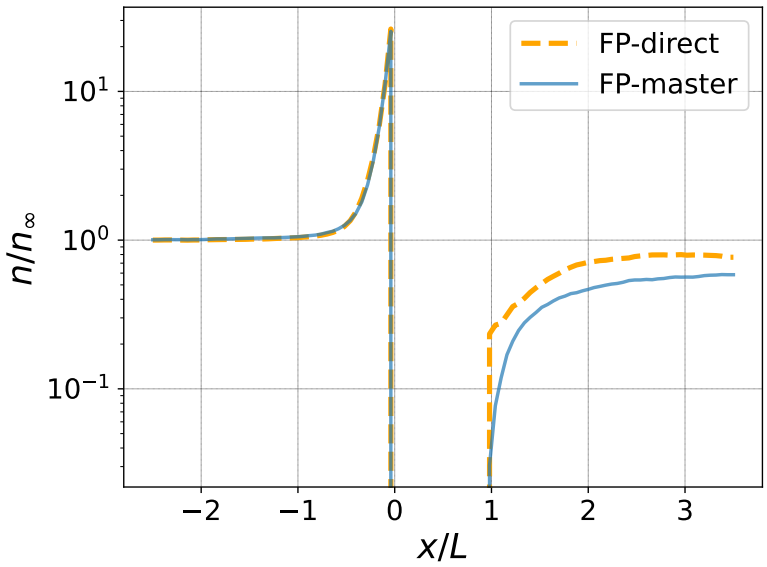

Figure 4.14.: Normalized particle density plot of the flow field downstream through the stagnation point in figure 4.12, normalized by characteristic length given by the cylinder diameter L for CO_2.

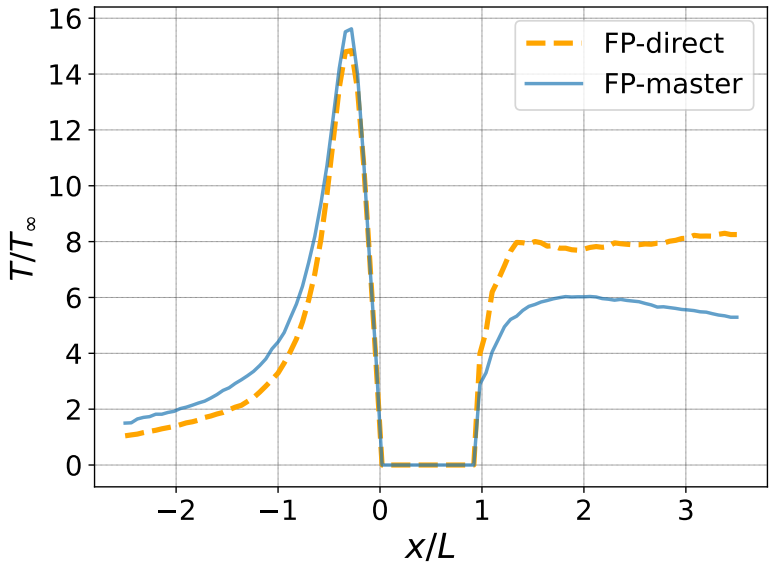

Figure 4.15.: Normalized temperature plot of the flow field downstream through the stagnation point in figure 4.13, normalized by characteristic length given by the cylinder diameter L for CO_2.

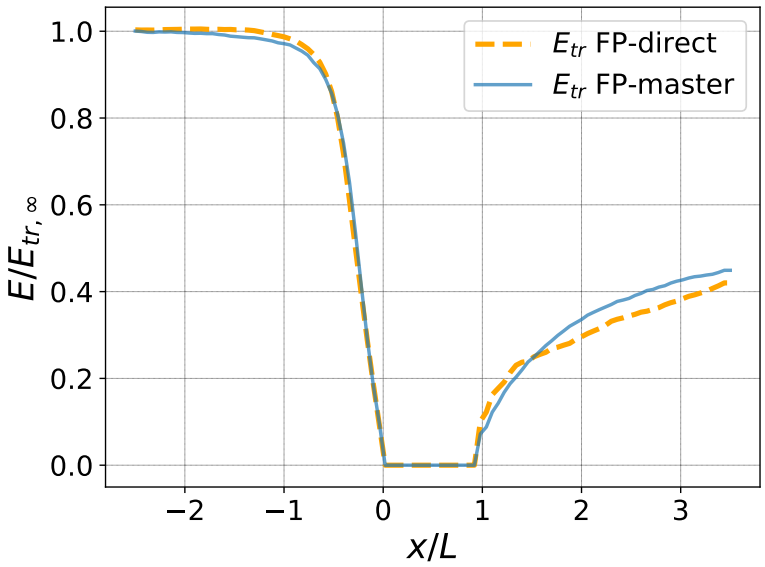

Figure 4.16.: Normalized translational energy plot of the flow field through the stagnation point in figure 4.13, normalized by characteristic length given by the cylinder diameter L for CO_2.

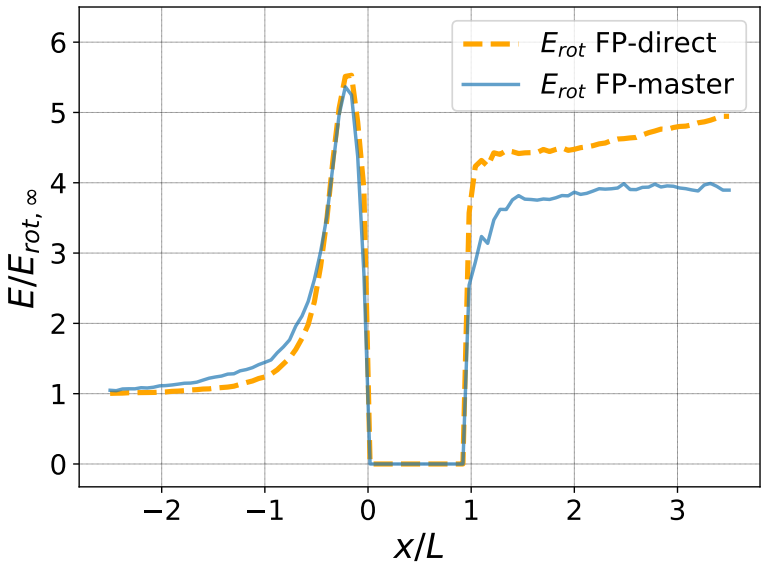

Figure 4.17.: Normalized rotational energy plot of the flow field through the stagnation point in figure 4.13, normalized by characteristic length given by the cylinder diameter L for CO_2.

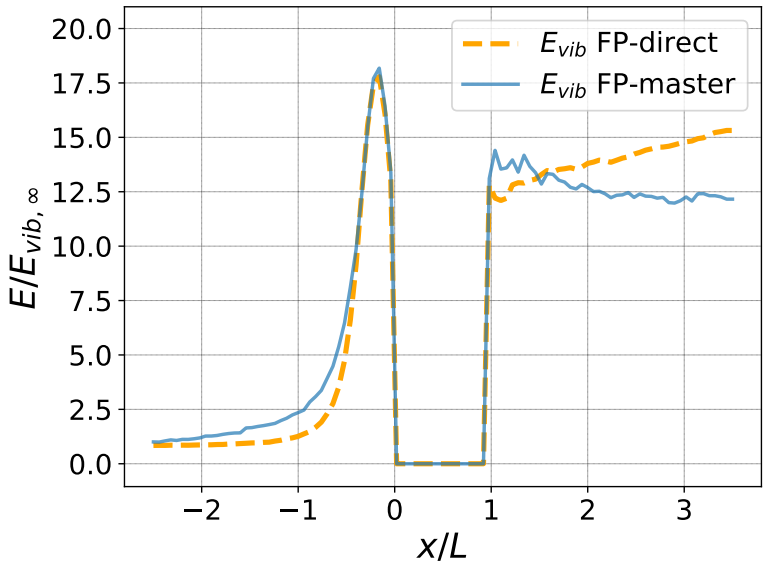

Figure 4.18.: Normalized vibrational energy plot of the flow field downstream through the stagnation point in figure 4.13, normalized by characteristic length given by the cylinder diameter L for CO_2.

4.3. Runtime efficiency

This section focuses on an investigation of the computation time of DSMC and FP modeling. As discussed in the section 3.3.1, the DSMC method becomes computationally very expensive for decreasing Knudsen numbers, due to the resolution criteria. These restrictions do not account for the FP modeling, which therefore provides an efficient modeling method for these crucial regions. Depending on a very hard to define switching criteria, either of the two methods is used to evaluate the new velocities in the simulation cell. The main goal will be a hybrid coupling of the DSMC with the FP method within a single simulation, which is beyond the scope of this thesis and left for future work.
The subsequent sections will take a look at the runtime of DSMC and FP for varying Knudsen numbers in section 4.3.1 and investigates how FP can also recover the temporal relaxation for larger timestep sizes in section 4.3.2 than the man collision time.

4.3.1. Varying Knudsen numbers

This section compares the runtime of DSMC with the FP direct modeling approach extended in this thesis and the FP master equation approach for varying Knudsen numbers. For both methods, DSMC and FP, simulations of smaller Knudsen numbers do not need to simulate more particles. Instead, smaller Knudsen numbers are modeled by DSMC with performing more collisions, whereas FP adjusts its model parameters. So for smaller Knudsen numbers, the number of calculations of pairwise collisions by DSMC increase dramatically. The FP model performs a constant number of computations for varying Knudsen numbers and it assigns new velocities to each particle in every timestep independently of the Knudsen number.
The runtime of the models will be compared by simulating particles in a box at different Knudsen numbers, using the length of the simulation box l as characteristic length of the Knudsen number $Kn = \lambda/l$. The weighting factor will be adjusted for the different Knudsen numbers, such that a constant number of 5000 particles is maintained. The particles are initialized in equilibrium with a temperature of $T = 300$ K. The results are averaged over 50 runs for each method at each Knudsen number and are shown in figures 4.19 and 4.20. The average runtimes are normalized with the averaged runtime of the FP direct modeling runs at $Kn = 0.1$. Note that this investigation only compares the runtime of the collision modeling, while molecular scales are not resolved as would be required by the DSMC resolution criteria. But a comparison with resolved resolution would be difficult to compare, since these restrictions do to account for FP [11]. The timestep size is chosen to resolve the reference Knudsen number of $Kn = 0.1$, but it is not adjusted for the different Knudsen numbers. The number of computations within a single timestep remain constant for different timestep sizes by the FP modeling. Therefor, a larger timestep requires fewer timestep samples for a fixed physical simulation time, which results in fewer total calculations. The accuracy of a timestep variation in the FP model is inverstigated in section 4.3.2.
For DSMC on the other hand, more collisions occur physically for smaller Knudsen numbers, but fewer collisions within a single timestep, if the timestep is adjusted to be smaller. So with a smaller timestep size, the number of collisions within a single timestep decreases, but more sample through time need to be performed to model the same simulation time, which obviously physically necessary leads to the same number of calculations of collisions, that are performed and timed in the end anyway. Therefore, also the timestep size remains constant for the different Knud-

sen numbers and only the computation time of the collision modeling is compared. Choosing the reference timestep size is done arbitrarily and the choice of a different timestep sizes for all simulations will shift the curves along the Knudsen number axis. This effectively influences only the DSMC curve and will shift the intersection point of the DSMC curve with the FP curves. Therefore, the results have to be considered carefully and may not be used to determine a switching criteria for the hybrid DSMC-FP coupling.
The runtime for the DSMC and the two FP methods as shown in figures 4.19 and 4.20 fulfill the expectation. They show a vastly increasing simulation time for the DSMC method with decreasing Knudsen numbers, whereas the computation times for the two FP methods remain approximately constant. It also reveals, that the FP modeling using the master equation approach from section 3.5 is almost twice as fast for N_2 and even a little bit more than twice as fast for CO_2 than using the direct modeling approach of the FP method. This is due to the fact that the direct modeling explicitly models the relaxation of each degree of freedom by an additional integration step, whereas the master equation approach directly generates the new particle energy from the rate coefficients.
For the specific test cases, the results show that for N_2 the FP direct modeling becomes more efficient than DSMC for Knudsen numbers smaller than $Kn < Kn_{\text{crit}} \approx 0.02$. The FP master equation modeling becomes already more efficient than DSMC for Knudsen numbers smaller than $Kn < Kn_{\text{crit}} \approx 0.05$. For CO_2, the critical Knudsen numbers shift and the FP methods become more efficient than DSMC for $Kn < Kn_{\text{crit}} \approx 0.01$ for the FP direct modeling and $Kn < Kn_{\text{crit}} \approx 0.02$ for the FP master equation modeling.
This critical Knudsen number depends on many parameters, like for example on the species and varying temperatures, which influence differential cross sections and the collision frequency.

4.3.2. Varying timestep sizes

This section recaps the temporal relaxation tests of the direct FP model for timestep sizes larger than the mean collision time. As already mentioned in previous sections, DSMC requires to resolve the mean collision time, which does not account for the FP modeling [12]. Therefore, FP can use larger timesteps to sample through the simulations, which provides a speed up in computation time. To perform the investigation, the relaxation of translational and internal energies of N_2 and CO_2 are

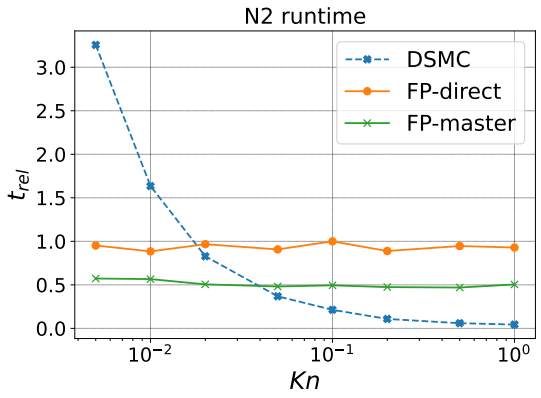

Figure 4.19.: Normalized relative runtime $t_{\text{rel}} = t/t_{\text{FP-direct},Kn=0.1}$ for N_2 with DSMC modeling of pairwise collisions and the FP methods modeling via drift and diffusion.

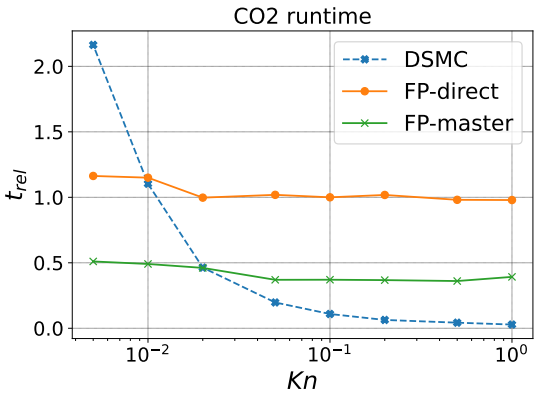

Figure 4.20.: Normalized relative runtime $t_{\text{rel}} = t/t_{\text{FP-direct},Kn=0.1}$ for CO_2 with DSMC modeling of pairwise collisions and the FP methods modeling via drift and diffusion.

investigated again, but with timestep sizes of $\Delta t = 0.3\tau_{\text{coll}}, 1\tau_{\text{coll}}, 2\tau_{\text{coll}}, 4\tau_{\text{coll}}$. For both species, the energies are initialized with energy values corresponding to temperatures of $T_{\text{tr}} = 9000$ K, $T_{\text{rot}} = 3000$ K and $T_{\text{vib}} = 4000$ K. The results are shown in figure 4.21 and 4.22. The results show, that the relaxation of the energies with larger timestep sizes than the mean collision time are recovered very well. Even a timestep size of $\Delta t = 4\tau_{\text{coll}}$ recovers the relaxation quite well, besides that it relaxes the energies a litte bit too fast. Larger timestep sizes, including $\Delta t = 4\tau_{\text{coll}}$, generally may not be able to resolve the temporal relaxation properly, because too few points are sampled anyway. The results also show large improvements to the corresponding previously published paper [18], by including the exact energy conservation factor in section 3.8 from further development between the time the paper has been published and this thesis was written.

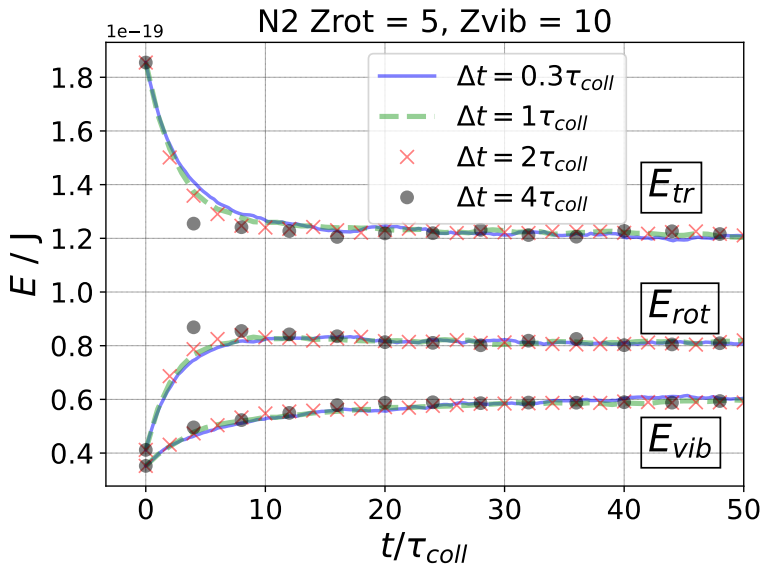

Figure 4.21.: Relaxation of translational, rotational and vibrational energy initialized at non-equilibrium energies for different timestep sizes Δt for N_2.

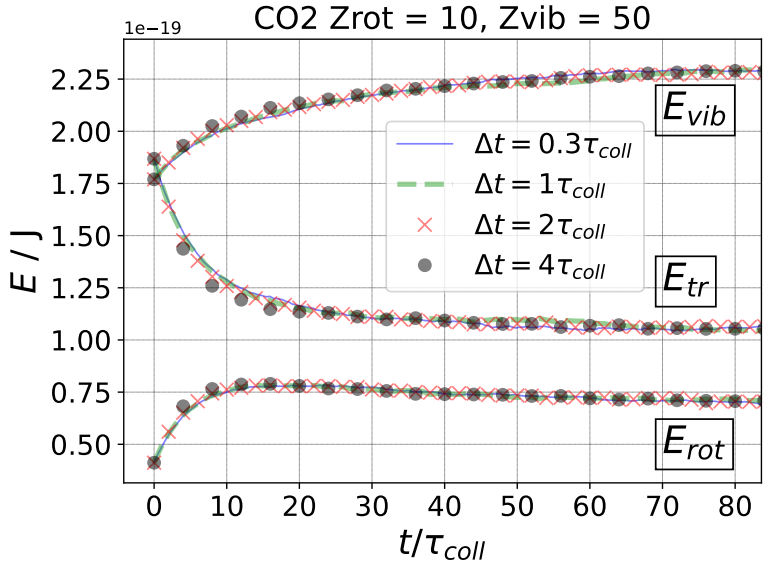

Figure 4.22.: Relaxation of translational, rotational and vibrational energy initialized at non-equilibrium energies for different timestep sizes Δt for CO_2.

5. Conclusion and outlook

The direct model approach of the diatomic model by Gorji et al. [6] has been extended to a polyatomic model in this Master's thesis. The model equations have been extended and build into a Fokker-Planck (FP) approximation of the collision term in the Boltzmann-equation. The energies are restricted to distribute on translational, rotational and vibrational modes and therefore do not include electron excitation energy, which requires a separate modeling method. The model is implemented as an additional collision model into the open source DSMC solver SPARTA [20]. The model can be used to perform full simulations but primarily may be used in a hybrid coupling with other particle simulation methods.
The goal of the FP model was to provide a model for regions of large densities where DSMC becomes computationally too expensive and unfeasible. To model the change of positions and velocities in time, DSMC calculates pairwise collisions which at larger densities results in more computational operations per timestep, due to a larger number of collisions in dense regions. The FP model computes the velocity change by local quantities like drift and diffusion where the computational effort is independent of the density and a constant number of velocity change calculations are performed. Therefore, it has been shown that there is a critical particle density at which the FP approximation becomes computationally more efficient than DSMC for larger densities.

The model is validated in accuracy and efficiency. In a first study, the relaxation of the model from non-equilibrium into equilibrium is investigated. A box with particles initialized with non-equilibrium energies of translational, rotational and vibrational modes and its relaxation in time is simulated. Here, the translational energy is only given by the thermal temperature of the particles and no additional velocity is added. A diatomic species of N_2 and polyatomic species of CO_2 and CH_4 are used. Energies and temperatures are plotted and compared to results from already validated reference data of DSMC and FP methods. All relaxation results

show good agreements with the corresponding reference data, estimating the equilibrium values very well and showing correct temporal relaxation.

A second study is performed for a hypersonic two dimensional flow around a cylinder at $Kn = 0.25$ and $Ma = 10$ where translational energy includes additional translational velocities to the thermal velocities. Two tests are performed, the first with a diatomic species of N_2 and the second one with a polyatomic species of CO_2. Both use equal wall temperature and free stream temperatures for all modes. The diatomic results show only small deviations and the model can be validated. The particle density is estimated very accurately and only a small overestimation in the stagnation point is observed. The peak value of the thermal temperature is estimated very well, while small spacial deviations can be observed. The shock thickness is a little bit larger and the maximum temperature value is a little bit closer to the body than predicted by the DSMC results. A study by Lofthouse et al. in 2008 [15] compared DSMC with CFD which also estimated the temperature maximum of the CFD results closer to the body than the DSMC results. This appears to be consistent with the expectation by fitting the FP model to the continuum limit. The small temporal deviations in the relaxation tests lead to a slight overestimation of the peak in rotational temperature in the shock. Vibrational energy is not excited in this test.
The polyatomic 2D tests show overall good agreement of the particle number density in the flow field and lineplots with small deviations in the wake region. The temperature field also shows good agreement from the free stream throughout the shock region but shows deviations in the wake regions. In the wake, the internal energies are overestimated which results in a too large temperature.

The last set of tests validate the efficiency of computation time of the FP approximation. It compares the runtime of the FP direct modeling approach and the FP master equation approach with the DSMC modeling. In a first study, a heat bath is simulated at different Knudsen numbers and the runtime is tracked and averaged over multiple runs for N_2 and CO_2. The results fully validate the expectations and show that both FP models remain a constant simulation time for varying Knudsen numbers while the DSMC runtime increases for smaller Knudsen numbers. Overall, the FP master equation approach is computationally about twice as fast as the FP direct modeling. As expected, the DSMC runtime changes from being more efficient

than both FP models for large Knudsen numbers to less efficient than both FP models for small Knudsen numbers. The second study of the last tests validate that additional computational efficiency can be gained by the FP direct modeling by remaining very accurate results even for larger timestep sizes than the mean collision time.

To sum it up, the test cases validate the extension for the FP direct modeling as a good model in terms of an accurately and efficiently approximating model. The model correctly relaxes the energies in polyatomic gases and the overall flow field is recovered well with only small deviations in free stream throughout the shock region. Larger deviations occur in the wake, where the gas is rarefied. With fitting the FP direct model to the continuum limit increasing deviations in rarefied regions are expected and observed in the tests. In a hybrid coupling approach, these rarefied regions may be modeled by an accurate DSMC model more efficiently anyway.
Further work may improve the spacial deviations of the energy for rarefied regions. Despite the deviations, the FP direct model can be used in a hybrid coupling to perform accurate and efficient reentry or jet plume simulations. So the main goal of providing a suitable polyatomic method for proper hybrid coupling with DSMC is fulfilled.

A. Model appendix

A.1. System of equations for the polyatomic cubic drift coefficient

As derived in [10], the model coefficients of the cubic drift coefficients c_{ij} and γ_i are determined by two considerations. The terms adding to a linear drift coefficients need to vanish to the second order moment:

$$c_{il}\overline{u_j' u_l'} + c_{jl}\overline{u_i' u_l'} + \gamma_i \overline{u_l' u_l' u_j'} + \gamma_j \overline{u_l' u_l' u_i'} + 2\Lambda \overline{u_i' u_j' u_k' u_k'} = 0, \tag{A.1}$$

and the translational heat flux need to match the heat flux of the *17-moment equation* [17]:

$$\begin{aligned} &-\frac{3}{\tau} q_{\mathrm{tr},i} + c_{il} q_{\mathrm{tr},l} + \rho c_{jl} \overline{u_j' u_l' u_i'} + \frac{\rho}{2}\gamma_i (\overline{u_l' u_l' u_j' u_j'} - \overline{u_l' u_l'}\ \overline{u_j' u_j'}) \\ &+ \rho \gamma_l (\overline{u_l' u_i' u_j' u_j'} - \overline{u_l' u_i'}\ \overline{u_j' u_j'}) + \frac{3\rho}{2}\Lambda \overline{u_i' u_j' u_j' u_l'} \\ =& -q_{\mathrm{tr},i}\left(\frac{16n}{15}\right) J_5 + \left(\frac{5nk_B}{3}\right)\left(\frac{J_1^{\mathrm{rot}}}{c_{\mathrm{rot}}} q_{\mathrm{rot},i} + \frac{J_1^{\mathrm{vib}}}{c_{\mathrm{vib}}} q_{\mathrm{vib},i}\right), \end{aligned} \tag{A.2}$$

with the mass density ρ, the particle density n and the Boltzmann constant k_B, while the right hand side revels the influence of the internal states like the internal heat capacities of rotation c_{rot} and vibration c_{vib} and internal heat fluxes $q_{\mathrm{rot},i}$ and $q_{\mathrm{vib},i}$, respectively. There, J_1 and J_5 are defined by

$$J_1^{\mathrm{int}} = \frac{2}{5}\left(\frac{5}{4}\frac{c_{\mathrm{int}}}{nk_B\tau_{\mathrm{int}}}\right), \quad \mathrm{int} \in \{\mathrm{rot}, \mathrm{vib}\} \tag{A.3}$$

$$J_5 = \frac{1}{4}\left(\frac{5}{2}\frac{k_B T}{\mu} + \frac{25}{12nk_B}\left(\frac{c_{\mathrm{rot}}}{\tau_{\mathrm{rot}}} + \frac{c_{\mathrm{vib}}}{\tau_{\mathrm{vib}}}\right)\right). \tag{A.4}$$

A.2. Derivation of internal diffusion coefficient

This section summarizes the calculation of the internal diffusion coefficients for rotation and vibration as needed by the FP model in section 3.6.3, following a suggested procedure proposed in [6]. The calculation is exemplary performed for rotation and can be transferred analogously to the derivation of the vibrational diffusion coefficient.

To model the internal states like rotation by the Fokker-Planck equation in the same way as translational velocities are modeled, rotational velocities Ω_i will be defined with the energy of the rotational mode i defined as $E_{\mathrm{rot},i} = I_i\overline{\Omega_i\Omega_i}/2$ with $\overline{(\cdot)} = \int_{\mathcal{H}}(\cdot)f\mathrm{d}\Psi$ using the moment of inertia of I_i around a rotational axis and the Einstein's index summation notation.
With the generalized model from section 3.6.1, the probability density function f is extended to $f(\mathbf{v}, \mathbf{\Omega}, \mathbf{\Xi}, \mathbf{x}, t)$ and the generalized FP equation can be written as

$$\left(\frac{\mathrm{D}}{\mathrm{D}t} + F_i\frac{\partial}{\partial v_i} + \frac{\partial}{\partial\Psi_i}\left(A_i - \frac{1}{2}\frac{\partial}{\partial\Psi_i}D_{ij}\right)\right)f = 0. \tag{A.5}$$

The tensor D_{ij} has as defined in section 3.6.3 only diagonal entries and takes the form $(D^2_{\mathrm{tr}}, D^2_{\mathrm{tr}}, D^2_{\mathrm{tr}}, D^2_{\mathrm{rot},1}, D^2_{\mathrm{rot},2}, D^2_{\mathrm{rot},3}, D^2_{\mathrm{vib},1}, ..., D^2_{\mathrm{vib,J}})$.
In a first step, equation (A.5) is multiplied by the internal energy, so $E_{\mathrm{rot},i} = I_i\Omega_i\Omega_i/2$

$$\left(\frac{\mathrm{D}}{\mathrm{D}t} + F_i\frac{\partial}{\partial v_i} + \frac{\partial}{\partial\Psi_i}\left(A_i - \frac{1}{2}\frac{\partial}{\partial\Psi_i}D_{ij}\right)\right)\frac{1}{2}I_i\Omega_i\Omega_i f = 0 \tag{A.6}$$

$$\Leftrightarrow \frac{\mathrm{D}}{\mathrm{D}t}I_i\Omega_i\Omega_i f + F_i\frac{\partial}{\partial v_i}I_i\Omega_i\Omega_i f + \frac{\partial}{\partial\Psi_i}A_iI_i\Omega_i\Omega_i f - \frac{1}{2}\frac{\partial^2}{\partial^2\Psi_i}D_{ij}I_i\Omega_i\Omega_i f = 0. \tag{A.7}$$

The rotational velocity is independent of the translational and vibrational velocity, i.e. $\Omega_i \neq \Omega_i(v_i)$ and $\Omega_i \neq \Omega_i(\xi_i)$, so the second term and the non-rotational derivatives in the third and fourth term vanish. This shortens the equation to

$$\frac{\mathrm{D}}{\mathrm{D}t}I_i\Omega_i\Omega_i f + \frac{\partial}{\partial\Omega_i}A_{\mathrm{rot},i}I_i\Omega_i\Omega_i f - \frac{1}{2}\frac{\partial^2}{\partial^2\Omega_i}\underbrace{D_{\mathrm{rot},ij}}_{=D^2_{\mathrm{rot},i}}I_i\Omega_i\Omega_i f = 0. \tag{A.8}$$

Assuming that the rotational diffusion coefficient may depend on the total temperature but not on the rotational velocity explicitly, i.e. $D_{\mathrm{rot},i} \neq D_{\mathrm{rot},i}(\Omega_i)$, the

rotational diffusion coefficient can be considered as a constant factor when applying the derivatives. This leads to the second term $\frac{\partial}{\partial\Omega_i}A_{\mathrm{rot},i}I_i\Omega_i\Omega_i f = 2I_iA_{\mathrm{rot},i}\Omega_i f$ and the third term can be calculated to $\frac{1}{2}\frac{\partial^2}{\partial^2\Omega_i}D^2_{\mathrm{rot},i}I_i\Omega_i\Omega_i f = I_iD^2_{\mathrm{rot},i}f$.
In a next step, the equation will be integrated over its phase space $\int_{\mathcal{H}}\mathrm{d}\Psi$ and it will be further assumed that the rotational diffusion generally does not depend on any phase space coordinates $D_{\mathrm{rot},i} \neq D_{\mathrm{rot},i}(\Psi_i)$

$$\int_{\mathcal{H}}\frac{\mathrm{D}}{\mathrm{D}t}I_i\Omega_i\Omega_i f\mathrm{d}\boldsymbol{\Psi} + \int_{\mathcal{H}}2I_iA_{\mathrm{rot},i}\Omega_i f\mathrm{d}\boldsymbol{\Psi} - \int_{\mathcal{H}}I_iD^2_{\mathrm{rot},i}f\mathrm{d}\boldsymbol{\Psi} = 0 \tag{A.9}$$

$$\Leftrightarrow \underbrace{\frac{\mathrm{D}}{\mathrm{D}t}I_i\underbrace{\int_{\mathcal{H}}\Omega_i\Omega_i f\mathrm{d}\boldsymbol{\Psi}}_{=\overline{\Omega_i\Omega_i}}}_{=2E_{\mathrm{rot},i}} + 2I_i\int_{\mathcal{H}}A_{\mathrm{rot},i}\Omega_i f\mathrm{d}\boldsymbol{\Psi} - I_iD^2_{\mathrm{rot},i}\underbrace{\int_{\mathcal{H}}f\mathrm{d}\boldsymbol{\Psi}}_{=1} = 0. \tag{A.10}$$

The rotational drift coefficient will be proposed to be linear in the rotational velocity Ω_i but independent of translational and vibrational velocities. So the integrals in the second term can be split up into:

$$2I_i\int_{\mathcal{H}}A_{\mathrm{rot},i}\Omega_i f\mathrm{d}\boldsymbol{\Psi} = 2I_i\int_{\mathbb{R}^3}\int_{\mathbb{R}^{d_{\mathrm{rot}}}}\int_{\mathbb{R}^{d_{\mathrm{vib}}}}A_{\mathrm{rot},i}\Omega_i f\mathrm{d}\mathbf{v}\mathrm{d}\boldsymbol{\Omega}\mathrm{d}\boldsymbol{\Xi} \tag{A.11}$$

$$= 2I_i\int_{\mathbb{R}^{d_{\mathrm{rot}}}}A_{\mathrm{rot},i}\Omega_i\underbrace{\int_{\mathbb{R}^3}\int_{\mathbb{R}^{d_{\mathrm{vib}}}}f\mathrm{d}\mathbf{v}\mathrm{d}\boldsymbol{\Xi}}_{=\int f(\boldsymbol{\Psi};\mathbf{x},t)\mathrm{d}\mathbf{v}\mathrm{d}\boldsymbol{\Xi}\equiv f(\boldsymbol{\Omega};\mathbf{x},t)}\mathrm{d}\boldsymbol{\Omega} \tag{A.12}$$

with the marginal probability function $f(\boldsymbol{\Omega};\mathbf{x},t)$ and using that $A_{\mathrm{rot},i} \neq A_{\mathrm{rot},i}(\mathbf{v},\boldsymbol{\Xi})$ and $\Omega_i \neq \Omega_i(\mathbf{v},\xi)$. Revisiting equation (A.10) using equation (A.12) for the second term, multiplying by a factor of $\frac{1}{2}$, and balancing the temporal change of $\mathrm{d}E_{\mathrm{rot},i}$ with the second and third term, leads to

$$\frac{\mathrm{d}E_{\mathrm{rot},i}}{\mathrm{d}t} = -I_i\int_{\mathbb{R}^{d_{\mathrm{rot}}}}A_{\mathrm{rot},i}\Omega_i f(\boldsymbol{\Omega};\mathbf{x},t)\mathrm{d}\boldsymbol{\Omega} + \frac{1}{2}I_iD^2_{\mathrm{rot},i}. \tag{A.13}$$

Choosing a rotational drift coefficient of $A_{\mathrm{rot},i} = \frac{1}{2\tau_{\mathrm{rot},i}}\Omega_i$, the eqution can be further calculated to

$$\frac{\mathrm{d}E_{\mathrm{rot},i}}{\mathrm{d}t} = -I_i \int_{\mathbb{R}^{d_{\mathrm{rot}}}} \frac{1}{2\tau_{\mathrm{rot},i}} \Omega_i \Omega_i f(\mathbf{\Omega}; \mathbf{x}, t) \mathrm{d}\mathbf{\Omega} + \frac{1}{2} I_i D_{\mathrm{rot},i}^2 \tag{A.14}$$

$$= -\frac{1}{\tau_{\mathrm{rot},i}} \frac{1}{2} I_i \underbrace{\int_{\mathbb{R}^{d_{\mathrm{rot}}}} \Omega_i \Omega_i f(\mathbf{\Omega}; \mathbf{x}, t) \mathrm{d}\mathbf{\Omega}}_{=\overline{\Omega_i \Omega_i}} + \frac{1}{2} I_i D_{\mathrm{rot},i}^2 \tag{A.15}$$

$$= -\frac{1}{\tau_{\mathrm{rot},i}} \underbrace{\frac{1}{2} I_i \overline{\Omega_i \Omega_i}}_{=E_{\mathrm{rot},i}} + \frac{1}{2} I_i D_{\mathrm{rot},i}^2 \tag{A.16}$$

$$= -\frac{1}{\tau_{\mathrm{rot},i}} E_{\mathrm{rot},i} + \frac{\tau_{\mathrm{rot},i}}{\tau_{\mathrm{rot},i}} \frac{1}{2} I_i D_{\mathrm{rot},i}^2 \tag{A.17}$$

$$= -\frac{1}{\tau_{\mathrm{rot},i}} \left(E_{\mathrm{rot},i} + \tau_{\mathrm{rot},i} \frac{1}{2} I_i D_{\mathrm{rot},i}^2 \right), \tag{A.18}$$

which comparing to the demanded *Landau-Teller* relaxations determines the equilibrium energy

$$\frac{\mathrm{d}E_{\mathrm{rot},i}}{\mathrm{d}t} = -\frac{1}{\tau_{\mathrm{rot},i}} \left(E_{\mathrm{rot},i} + \underbrace{\tau_{\mathrm{rot},i} \frac{1}{2} I_i D_{\mathrm{rot},i}^2}_{\stackrel{!}{=} E_{\mathrm{rot,i}}^{\mathrm{eq}}} \right). \tag{A.19}$$

The equilibrium energy for a given temperature generally can be calculated as shown in section 2.2.5 and therefore can be used to determine the diffusion coefficient for each independent rotational degree of freedom

$$E_{\mathrm{rot,i}}^{\mathrm{eq}} = \tau_{\mathrm{rot},i} \frac{1}{2} I_i D_{\mathrm{rot},i}^2 \tag{A.20}$$

$$\Leftrightarrow D_{\mathrm{rot},i} = \sqrt{\frac{2E_{\mathrm{rot,i}}^{\mathrm{eq}}}{I_i \tau_{\mathrm{rot},i}}}. \tag{A.21}$$

Performing the same calculation by replacing the rotational energy $E_{\mathrm{rot},i}$ by a vibrational energy defined as $E_{\mathrm{vib},i} = \overline{\Xi_i \Xi_i}/2$ dropping the moment of inertia I_i and with the exchange of $\Omega_i \to \Xi_i$, will lead to the diffusion coefficient for each independent vibrational mode depending on the vibrational equilibrium energy by

$$E_{\mathrm{vib,i}}^{\mathrm{eq}} = \tau_{\mathrm{vib},i} \frac{1}{2} D_{\mathrm{vib},i}^2 \Leftrightarrow D_{\mathrm{vib},i} = \sqrt{\frac{2E_{\mathrm{vib,i}}^{\mathrm{eq}}}{\tau_{\mathrm{vib},i}}}. \tag{A.22}$$

A.3. Numerical routine

Translating the modeling and its integration schemes of equations (3.39), (3.41) and (3.42) into code has been done as briefly shown by the pseudocode routine in algorithm 1. The implementation of the Fokker-Planck algorithm has been done into the DSMC SPARTA code [20]. Attention has to be payed to the correct ordering of the functions. It is important to fully relax all internal states and update the internal energies before updating the translational energies, to get the correct scaling for the energy conservation factor by equation (3.8). Therefore, values of old and updated states need to be kept, in order to properly rescale the tranlsational velocity change. There are a variety of implementation details that had to be taken care of, but will not be further discussed at this point.

Algorithm 1 Summarized routine of Fokker-Planck collision operation

$v_{\mathrm{rot},i},\ v_{\mathrm{vib},i} \leftarrow$ INITIALIZE$(E_{\mathrm{rot},i}, E_{\mathrm{vib},i})$

for $k = 1, ..., N_{\mathrm{cell}}$ **do**

  $\rho_k \leftarrow$ CALCULATE DENSITY

  $p_k \leftarrow$ CALCULATE PRESSURE

  $\nu_k \leftarrow$ CALCULATE VISCOSITY

  $E^n_{\mathrm{rot}}, E^n_{\mathrm{vib}} \leftarrow$ CALCULATE OLD AVERAGE INTERNAL ENERGIES$(E^n_{\mathrm{rot},i}, E^n_{\mathrm{vib},i})$

  CALCULATE ALL TAU$(\tau_{\mathrm{coll}}, \tau_{\mathrm{tr}}, \tau_{\mathrm{rot}}, \tau_{\mathrm{vib},i})$

  CALCULATE INTERNAL DIFFUSION COEFFICIENTS$(D_{\mathrm{rot},i}, D_{\mathrm{vib},i})$

  $v^{n+1}_{\mathrm{rot},i},\ v^{n+1}_{\mathrm{vib},i} \leftarrow$ PROPAGATE INTERNAL VELOCITIES$(v^n_{\mathrm{rot},i},\ v^n_{\mathrm{vib},i})$

  $E^{n+1}_{\mathrm{rot},i}, E^{n+1}_{\mathrm{vib},i} \leftarrow$ CALCULATE NEW INTERNAL ENERGIES$(v^{n+1}_{\mathrm{rot},i},\ v^{n+1}_{\mathrm{vib},i})$

  $E^{n+1}_{\mathrm{rot}}, E^{n+1}_{\mathrm{vib}} \leftarrow$ CALCULATE NEW AVE INT ENERGIES$(E^{n+1}_{\mathrm{rot},i}, E^{n+1}_{\mathrm{vib},i})$

  CALCULATE TRANSLATIONAL DIFFUSION COEFFICIENTS$(D_{\mathrm{tr},i})$

  $c_{ij}, \gamma_i \leftarrow$ SOLVE LINEAR SYSTEM OF EQUATIONS$(...)$

  $v^{n+1}_i \leftarrow$ PROPAGATE TRANSLATIONAL VELOCITIES(v^n_i)

  $\alpha \leftarrow$ CALCULATE SCALING FACTOR$(v^n_i, v^{n+1}_i, E^n_{\mathrm{rot}}, E^n_{\mathrm{vib}}, E^{n+1}_{\mathrm{rot},i}, E^{n+1}_{\mathrm{vib},i})$

  RESCALE TRANSLATIONAL VELOCITIES(v^{n+1}_i, α)

end for

B. Further study appendix

B.1. Theoretic prediction of rotational relaxation

To investigate if the model fulfills the *Landau-Teller* relaxation, the differential equation of the change of rotational energy in time is derived. Assuming a given constant total energy E_{tot} from translational and rotational energy with d_{rot} degrees of freedom, the total energy is given by $E_{\mathrm{tot}} = E_{\mathrm{tr}} + E_{\mathrm{rot}} = 3k_BT/2 + d_{\mathrm{rot}}k_BT/2$ and equal temperature defines the equilibrium energy $E^{\mathrm{eq}} = E_{\mathrm{rot}}(T)$. Therefore, the temperature is

$$T = \frac{2}{3k_B}\left(E_{\mathrm{tot}} - E_{\mathrm{rot}}\right), \tag{B.1}$$

which leads to the equilibrium energy

$$E^{\mathrm{eq}} = E_{\mathrm{rot}}(T) = \frac{d_{\mathrm{rot}}}{2}k_B\frac{2}{3k_B} = \frac{d_{\mathrm{rot}}}{3}(E_{\mathrm{tot}} - E_{\mathrm{rot}}). \tag{B.2}$$

With the *Landau-Teller* relaxation as defined by equation (3.20), the change of rotational energy is given by

$$\frac{\partial E_{\mathrm{rot}}}{\partial t} = \frac{E^{\mathrm{eq}} - E_{\mathrm{rot}}}{\tau} = \frac{1}{\tau}\left(\frac{d_{\mathrm{rot}}}{3}E_{\mathrm{tot}} - E_{\mathrm{rot}}\frac{d_{\mathrm{rot}}+3}{3}\right). \tag{B.3}$$

The change of translational energy is given by the balance to the total energy and can be calculated with a changing rotational energy by $E_{\mathrm{tr}} = E_{\mathrm{tot}} - E_{\mathrm{rot}}$.

B.2. A study of Lofthouse et al. comparing CFD and DSMC around a cylinder

A study of Lofthouse et al. in 2008 [15] compared DSMC with computational fluid dynamics (CFD) also with a flow around a cylinder at $Kn = 0.25$ and $Ma = 10$. They did not use equal free stream and wall temperature as in the tests in section 4.2.2 and used a monatomic gas of Argon. The comparison of the temperature field using DSMC and CFD is shown in figure B.1.

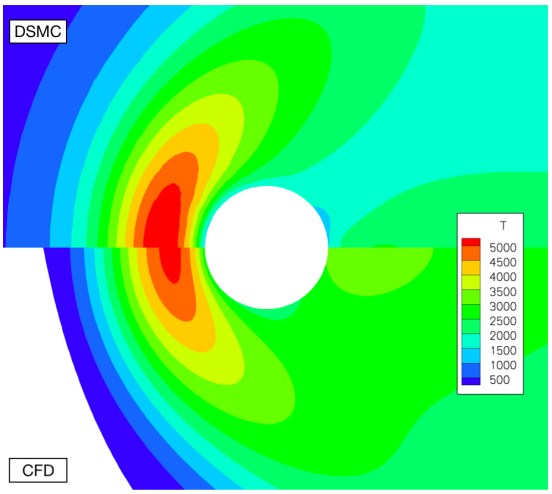

Figure B.1.: Temperature field comparing DSMC and CFD at $Kn = 0.25$ and $Ma = 10$ by Lofthouse et al. 2008 [15] using Argon.

Their results show, that the location of the maximum of the temperature field in the CFD solution is closer to the body than for the DSMC result. The FP solution in figure 4.7 also estimates the location of the maximum temperature closer to the body than DSMC. This fulfills well the expectation due to a matching of the FP production terms with the continuum limit. The shock thickness on the other hand is underestimated by CFD compared to DSMC, whereas FP overestimates the shock thickness.

Bibliography

[1] John David Anderson. Hypersonic and high-temperature gas dynamics second edition. *American Institute of Aeronautics and Astronautics*, 2006.

[2] Peter Atkins, Peter William Atkins, and Julio de Paula. *Atkins' physical chemistry*. Oxford university press, 2012.

[3] R Balian. From microphysics to macrophysics, vol. i, 1991.

[4] Leo Basov and Martin Grabe. Modeling of polyatomic gases in the kinetic fokker-planck method by extension of the master equation approach. In *32nd International Symposium on Rarefied Gas Dynamics 2022*, 2022.

[5] G.A. Bird. *Molecular Gas Dynamics and the Direct Simulation of Gas Flows*. Oxford Engineering Science Series, Clarendon Press, 1994.

[6] M Hossein Gorji and Patrick Jenny. A fokker–planck based kinetic model for diatomic rarefied gas flows. *Physics of fluids*, 25(6):062002, 2013.

[7] M Hossein Gorji and Patrick Jenny. An efficient particle fokker–planck algorithm for rarefied gas flows. *Journal of Computational Physics*, 262:325–343, 2014.

[8] M Hossein Gorji and Patrick Jenny. Fokker–planck–dsmc algorithm for simulations of rarefied gas flows. *Journal of Computational Physics*, 287:110–129, 2015.

[9] M Hossein Gorji and Manuel Torrilhon. Entropic fokker-planck kinetic model. *Journal of Computational Physics*, 430:110034, 2021.

[10] Mohammad H Gorji, Maniel Torrilhon, and Patrick Jenny. Fokker–planck model for computational studies of monatomic rarefied gas flows. *Journal of fluid mechanics*, 680:574–601, 2011.

[11] Christian Hepp, Martin Grabe, and Klaus Hannemann. A kinetic fokker–planck approach to model hard-sphere gas mixtures. *Physics of Fluids*, 32(2):027103, 2020.

[12] Christian Hepp, Martin Grabe, and Klaus Hannemann. Master equation approach for modeling diatomic gas flows with a kinetic fokker-planck algorithm. *Journal of Computational Physics*, 418:109638, 2020.

[13] MS Ivanov, GN Markelov, SF Gimelshein, LV Mishina, AN Krylov, and NV Grechko. High-altitude capsule aerodynamics with real gas effects. *Journal of Spacecraft and Rockets*, 35(1):16–22, 1998.

[14] Patrick Jenny, Manuel Torrilhon, and Stefan Heinz. A solution algorithm for the fluid dynamic equations based on a stochastic model for molecular motion. *Journal of computational physics*, 229(4):1077–1098, 2010.

[15] Andrew J Lofthouse, Leonardo C Scalabrin, and Iain D Boyd. Velocity slip and temperature jump in hypersonic aerothermodynamics. *Journal of thermophysics and heat transfer*, 22(1):38–49, 2008.

[16] Julien Mathiaud and Luc Mieussens. A fokker–planck model of the boltzmann equation with correct prandtl number for polyatomic gases. *Journal of Statistical Physics*, 168:1031–1055, 2017.

[17] Francis J McCormack. Kinetic equations for polyatomic gases: The 17-moment approximation. *The Physics of Fluids*, 11(12):2533–2543, 1968.

[18] Aaron Nagel, Leo Basov, and Martin Grabe. Modeling of polyatomic gas flows within a kinetic fokker-planck approach using a direct modeling method. *10th EUCASS-9th CEAS 2023*, 2023.

[19] Marcel Pfeiffer, Paul Nizenkov, and Stefanos Fasoulas. Extension of particle-based bgk models to polyatomic species in hypersonic flow around a flat-faced cylinder. In *AIP Conference Proceedings*, volume 2132, page 100001. AIP Publishing LLC, 2019.

[20] SJ Plimpton, SG Moore, A Borner, AK Stagg, TP Koehler, JR Torczynski, and MA Gallis. Direct simulation monte carlo on petaflop supercomputers and beyond. *Physics of Fluids*, 31(8):086101, 2019. doi: 10.1063/1.5108534. URL `http://sparta.sandia.gov`.

[21] CRAFT tech Combustion Research and Flow Technology. Space vehicle reentry, 2023. URL `https://www.craft-tech.com/applications/rockets-and-space-vehicles/space-vehicle-reentry/`.

[22] Huidan Yu. *Lattice Boltzmann equation simulations of turbulence,* mixing, and combustion.* Texas A&M University, 2004.

Acknowledgment

My greatest and sincere acknowledgment is to my supervisor Leo, who constantly highly motivated and supported me with his huge inside knowledge in the field, always able to answer all my questions, and making me deliver better. Also for all the sophisticated and casual discussions, on and off work, including colleagues from the department.

I want to thank Martin, for his insanely great empathy and talent in leading peoples work and finding just the right words to motivate when needed. Also for making me extremely interested in the field and often making me feel smater than I thought I was.

Finally, both my parents, for their constant, unconditioned support on my journey through all the years of my physics study.

Erklärung Ich versichere hiermit, dass ich die vorliegende Arbeit ohne fremde Hilfe selbstständig verfasst und nur die von mir angegebenen Quellen und Hilfsmittel verwendet habe. Wörtlich oder sinngemäß aus anderen Werken entnommene Stellen habe ich unter Angabe der Quellen kenntlich gemacht. Die Richtlinien zur Sicherung der guten wissenschaftlichen Praxis an der Universität Göttingen wurden von mir beachtet. Eine gegebenenfalls eingereichte digitale Version stimmt mit der schriftlichen Fassung überein. Mir ist bewusst, dass bei Verstoß gegen diese Grundsätze die Prüfung mit nicht bestanden bewertet wird.

Göttingen, den October 12, 2023

(Aaron Nagel)